NTNU

Norwegian University of
Science and Technology

Mathematical Modeling of Coalescence of Oil Droplets in Water Flow

Eirik Kufås

Master of Science in Energy and Environment
Submission date: June 2008
Supervisor: Kjell Erik Rian, EPT

Norwegian University of Science and Technology
Department of Energy and Process Engineering

Problem Description

Through this Master's thesis the goal is to study mathematical models for coalescence of oil droplets in a water flow. The industrial basis for this project is the need for a mathematical model that can be applied in CFD simulations for the optimization of swirl-based coalescers.
The project will be carried out in close cooperation with Aker Process Systems AS, Division of Advanced Separation.

The following tasks should be considered in the project work:

1. Carry out a literature review on liquid-liquid coalescence with special focus on oil droplet coalescence in a continuous water phase. Give a thorough discussion of the problem.

2. Formulate a mathematical model for coalescence of oil droplets in a water flow.

3. In cooperation with the advisors, select a suitable numerical simulation tool to study coalescence of oil droplets in a water flow. Give a description of the relevant parts of this program system.Perform relevant numerical simulations and discuss the results thoroughly.

4. If necessary, suggest further improvements of the mathematical model.

Assignment given: 01. February 2008
Supervisor: Kjell Erik Rian, EPT

Declaration

I hereby declare that this Master's thesis is prepared independently and according to the rules and regulations of NTNU as well as passive directions given by the Department of Energy and Process Engineering.

Oslo 27/06/08

_____

Eirik Kufås

Preface

This Master's thesis is carried out at the Department of Energy and Process Engineering, NTNU during the spring 2008. The project is carried out in cooperation with Aker Process Systems AS, Division of Advanced Separation.

I would like to thank my supervisors at NTNU during this Master thesis, Kjell Erik Rian, Maria Fernandino and Carlos Dorao for helpful advices during the work, as well as Morten Hana and Vishwas Dindore at Aker Process Systems AS for very interesting proposal for this Master assignment.

A special thanks goes to my good friends that I have been sharing working place with over the last year for keeping up a good mood throughout the whole period for this work.

Oslo 27/06/08

_____

Eirik Kufås

Abstract

Liquid-liquid coalescers are devices used for increasing the droplet size of the dispersed phase in continuous phase flow, such as oil droplets in water flow. The efficiency of separation technologies is strongly dependent on the droplet size, which is desirable to shift into larger droplet diameters. Theory behind coalescence and its modeling is studied in this Maser's thesis. Aker Process Systems AS, Division of Advanced Separation Technology, provided the assignment proposal.

The scope of this work is a literature study on the coalescence phenomenon and the closely related break-up phenomenon and CFD modeling in general. Further a mathematical model for simulating coalescence of oil droplets in continuous water flow is developed by the use of the commercial CFD-code FLUENT. The basis for the model is a swirl-based coalescer called Compact Tubular Coalescer (CTC), developed by Aker Process Systems AS.

The validity of the model is evaluated before different aspects of the performance of the coalescer are studied. Several validation criteria were tested and were acceptable, but some weaknesses regarding lack of test cases were detected. The performance testing showed good performance of the CTC, it was able to increase the Sauter Mean Diameter (SMD) of the droplet with up to 250% for the smallest droplets (20 μm) and highest volume fractions (7%). Remarkable differences of the performance were observed as the physical properties were changed. Higher viscosity and droplet surface tension lead to increased coalescence rate and decreased break-up rate.

Future work is recommended to concentrate on improving the present model and to investigate more aspects of the model. An effort should also be made to use a Eulerian approach to model the dispersed phase with the use of population balances, in order to be able to simulate flows with larger dispersed phase volume fractions.

Table of Contents

List of Figures

List of Tables

Nomenclature

Greek Symbols

α	Thermal diffusivity
α_p	Under-relaxation factor for pressure
Γ	Diffusion coefficient
γ	Drop size ratio
Δ	Diameter ratio/arithmetic difference
μ	Dynamic viscosity/micro-, 10^{-6}
ρ	Density
σ	Surface tension
$\sigma_{l,s}$	Collision cross section
$\bar{\tau}$	Stress tensor
ϕ	General flow variable

Latin Symbols

a	Acceleration
c	Speed of sound
A	Area/amplitude
$\vec{A}_f$	Area of face f
C	General coefficient
c_v	Heat capacity
c_0	Indication of cell 0
c_1	Indication of cell 1
d	Diameter
d_{32}	Sauter Mean Diameter (SMD)
F	Force
g	Gravitational acceleration
J_f	Mass flux through face f
k	Thermal conductivity
m	Mass
n	Number of droplets
N_{Vi}	Viscosity number for shear flows
N_{We}	Weber number for shear flows
p	Pressure
$P_{l,s}$	Probability of collision between droplets
S	Source term
t	Time
u	Velocity in x-direction
u_{rel}	Relative velocity between droplets

$\overline{v^2}$	Averaged square of the relative velocity between droplet and fluid
$\vec{v}$	Velocity vector
V_{col}	Collision volume
x	Impact parameter
X	Distance from one droplet to the relative velocity vector placed on the center of another droplet

Abbreviations

CFD	Computational Fluid Dynamics
CTC	Compact Tubular Coalescer
DPM	Discrete Phase Model
FVM	Finite Volume Method
Ma	Mach number
PDE	Partial Differential Equation
RANS	Reynolds-Averaged Navier-Stokes
Re	Reynolds number
RSM	Reynolds-Stress Equation Model
SMD	Sauter Mean Diameter
We	Weber number for particles

Indices

c	Continuous phase
crit	Critical
d	Dispersed phase
D	Drag
l	Large
p	Particle
rel	Relative
s	Small
Taylor	Taylor's analogy

1 Introduction

1.1 Motivation

The aim of oil and gas processing facilities is to process wellhead fluids into different products. These products are transported to the customer by e.g. ships, trailers or in pipelines. This processing of oil and/or gas for transportation or storage is called oilfield processing. But some of the processed fluids are not transported and sold; reinjection and disposal of fluids and gasses are usual. Therefore, oilfield processing also includes water treatment, which means cleaning of water that is to be used for disposal or reinjection. When it comes to disposal, environmental issues must be considered. This puts demands on the pureness of the water in order not to pollute the sea. This water contains small oil or other hydrocarbon droplets from the well stream, which need to be removed, thus separation equipment is needed.

For this purpose hydrocyclones and flash drums are often used as separation equipments. These separators have better performance with larger inlet size distribution of the oil droplets, which are to be separated out. In order to increase the diameter of the droplets that enter the separation device, a coalescer could be used. Coalescers are widely used in the oil and gas. A coalescer is a device where droplets of the dispersed phase are coalescing into larger drops that are more amenable to removal. Aker Process Systems AS suggested the topic of the present work; they are developing a product called Compact Tubular Coalescer (CTC™). The principle of the CTC is to force the droplets into a turbulence and centrifugal flow pattern by setting the fluid in rotation in a tube. The centrifugal forces will force the water to the outer walls while the lighter hydrocarbon will remain in the middle of the tube and coalesce. Mathematical models of the device are important in order to make the design as efficient as possible. This work focuses on coalescence of oil droplets in water. The CTC is used as a basis for the modeling of the coalescence phenomenon, and different aspects of the performance of the CTC is studied.

1.2 Introduction to Dispersed Two-Phase Flows

Dispersed flow occurs when one fluid is in the form of droplets within the continuum of the other fluid. There are numerous applications to this kind of flows, particularly in the separation part of the process industry where oil and water are exploited together and then need to be separated from each other. In turbulent dispersed flows, the droplets can interact with the turbulent eddies of the continuous phase in many different ways depending on the sizes of the droplets and eddies. This interaction can influence and change the structure and parameters of the turbulent flow. Thus, knowledge about the droplet size distribution in two-liquid mixture is necessary in order to be able to predict the final conditions in separation devices like the CTC and it will lead to better modeling and design of separation devices containing dispersed flows.

In turbulent dispersions, both breakup and coalescence usually take place continuously, and these processes will determine the final droplet size distribution.

1.3 Aim of the Present Work

The main purpose of this thesis is to describe and discuss the theoretical background for liquid-liquid coalescence, with special focus on coalescence of oil droplets in a continuum water phase, and then formulate a mathematical model of a case that includes such coalescence. As mentioned above, the performance of the CTC is used as the case of study in order to see how coalescence affects the separation performance, and which advantages the design of the CTC has. A commercial Computational Fluid Dynamics (CFD) code, FLUENT 6.3.26, is used to make simulations of the model, and GAMBIT 2.4 is used to make geometries and grids. The results are evaluated and discussed in order to find out how good the model is and which further improvements that should be made.

1.4 Structure of the Report

The report starts with a physical description of the phenomenon of liquid-liquid coalescence in dispersed two-phase turbulent flows. It begins with a general description of what coalescence is and how it occurs, before more details about collision between particles and the outcomes of the collisions are discussed (chapter 2). A description of the closely related break-up phenomenon is given in this chapter as well. This is followed by a closer look on CFD in general, and how regular continuous phase flows are treated in FLUENT. The numerical method used by FLUENT, the finite volume method (FVM), is described (chapter 3). Further, the modeling of particle collision, coalescence and break-up are treated and given a detailed description, and this is linked to how the CFD software, FLUENT, uses this model to predict collision, coalescence and break-up (chapter 4). A chapter with computational methodology and description of the simulations is given before results are presented and discussed. Some recommendations about further work are also given. Appendices and list of references are given in the end.

2 Physical Theory

2.1 Coalescence as a Phenomenon

Any multiphase process involves a multitude of interactions, and these interactions may involve collisions between droplets and particles. Coalescence occurs when two or more such particles collide and are in contact long enough. The collision is caused by spatial velocity differences between particles. The velocity differences may be caused by several factors. Prince & Blanch (1990) mention three mechanisms that can lead to collision:

- Turbulence: The length scale of the turbulent eddies that causes relative velocity differences between particles must be in the order of the diameter of the particle. If the eddies are too small, they will not contain enough energy to affect the particle motion. On the other hand, if the eddies are much larger than the size of the particle, ensembles of particles are transported together and do not affect the relative motion between them. Droplet collisions caused by velocity fluctuations are similar to the random movement of gas molecules in the kinetic gas theory.
- Buoyancy: Collision is caused by difference in the rise velocities of the particles with different size. Larger droplets can catch smaller ones on their way.
- Laminar shear: Collision occurs as a result of large circulation patterns in e.g. a tube.

Not every collision leads necessarily to coalescence. Several models exist for describing when collision leads to coalescence and when it does not. For coalescence to happen, the particles have to remain in contact with each other for long enough time for the liquid film between them to drain to the critical size necessary to break it. This is a common requirement for all models. This means that also the film's thinning rate is a parameter for occurrence of coalescence.

2.2 Collision between Particles

Dhainaut (2002) mentions the other possible outcomes from a collision; bouncing, separation and shattering. When the outcome is bouncing, the intervening film on the colliding particles' surfaces prevents coalescence and the particles bounce apart. In this case the drops may go through deformation, but there is no mass exchange. Separation collision occurs when two particles connect temporarily and separate immediately after into two or more drops. Shattering collision occurs when particles with high relative velocity collide and breaks into several smaller particles.

Ashgriz & Poo (1990) claim that the main parameters that control the outcome of a collision are the Weber number, the colliding particles' diameter ratio, the Reynolds number and the impact parameter, as presented in Eq. (2.1)-(2.4).

Weber number:

$$We = \frac{\rho d_s u_{rel}^2}{\sigma} \tag{2.1}$$

Diameter ratio:

$$\Delta = \frac{d_s}{d_l} \tag{2.2}$$

Impact diameter:

$$x = \frac{2X}{d_l + d_s} \tag{2.3}$$

Reynolds number:

$$\mathrm{Re} = \frac{\rho d_l u_{rel}}{\mu} \tag{2.4}$$

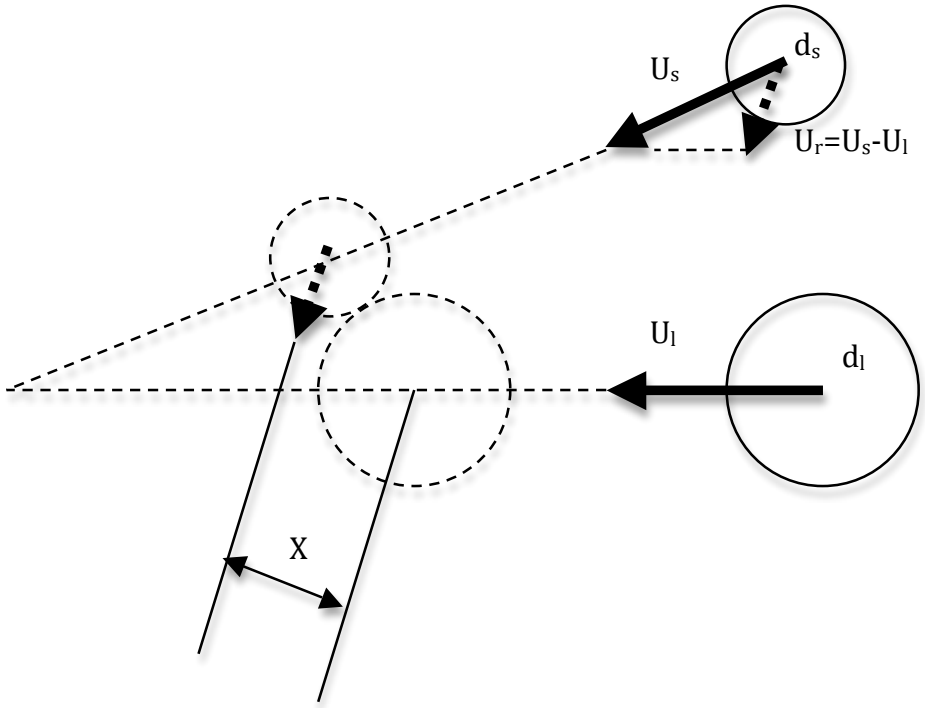

Fig. 2.1: Description of factors in the expression for the impact parameter.

The factors in the impact parameter for two colliding particles are shown in Fig. 2.1. X is the distance from the center of one drop to the relative velocity vector placed on the center of the other drop, while d_l and d_s are the diameters of the large and the small drop, respectively.

Ashgriz & Poo (1990) presented two possible types of separation collisions: reflexive separation and stretching separation. In reflexive separation a near head-on collision occurs between the two colliding particles (Fig. 2.2). In this separation the liquid inside the temporarily coalesced drop experiences a pressure difference between the two extremities and the center of the drop, which pushes the liquid from the center and then the drop separates into two new drops. When two drops of non-equal size collide the initial large drop loses

some mass to the small drop such that the small drop becomes the largest after the collision.

In stretching separation only a part of each drop is in direct contact with each other. The rest of the drops tend to continue to flow in their initial direction (Fig. 2.3). As a consequence, the region of interaction between the two drops is stretched. Thus, there are two competing forces involved in the collision: the surface tension in the region of interaction, which is holding the drops together (draining), and the kinetic energy of the initial drops, which is stretching the drops and separating them. For drops of different sizes the two competing forces will determine the size of the drops after the collision. The stretching effect will cause mass transfer from the small drop to the large drop, as for the reflexive separation, but the drainage effect will make the small drop scoop out some of the mass of the large drop because of lower internal pressure inside the large drop compared to the small drop.

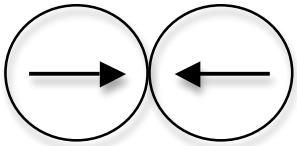

Fig. 2.2: Head-on collision between two particles (reflexive separation).

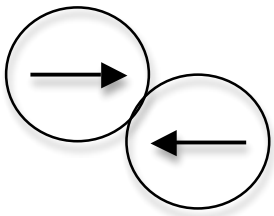

Fig. 2.3: Collision with partial region of interaction (stretching separation).

In both cases of separation, the outcome may usually result in several satellite drops. That means that the two colliding particles will produce two new particles, but also several smaller particles will arise (Fig. 2.4)

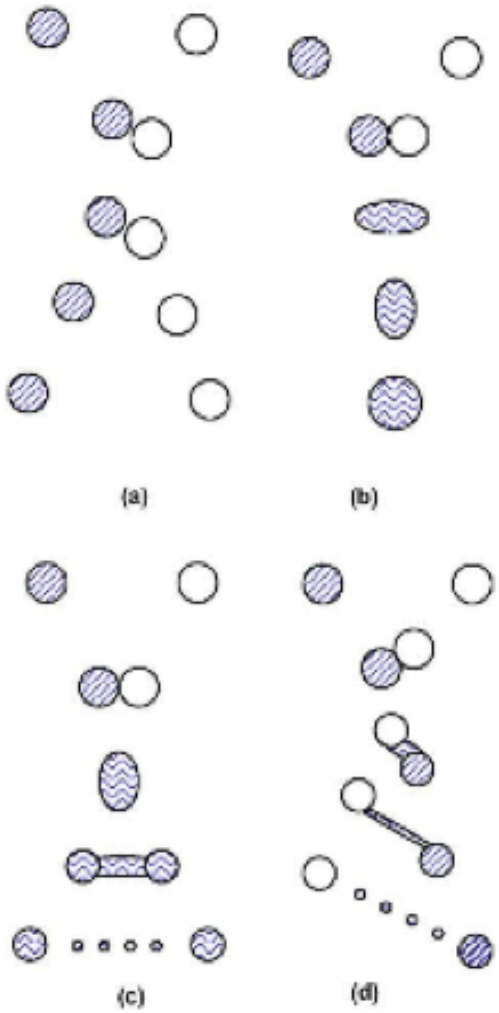

(a) bouncing; (b) coalescence; (c) reflexive separation; (d) strethcing separation

Fig. 2.4: Diagram of collision regimes (Ko & Ryou, 2005).

By relating the impact parameter to the two types of separation collisions, it appears that head-on collisions correspond to an impact parameter equal to zero, while for oblique collisions the impact parameter equals one.

Coalescence occurs for impact values between the ones for stretching and reflexive collisions. Analytical results based on experiments for when coalescence occurs are presented in Fig. 2.5 as a function of impact parameter and Weber number.

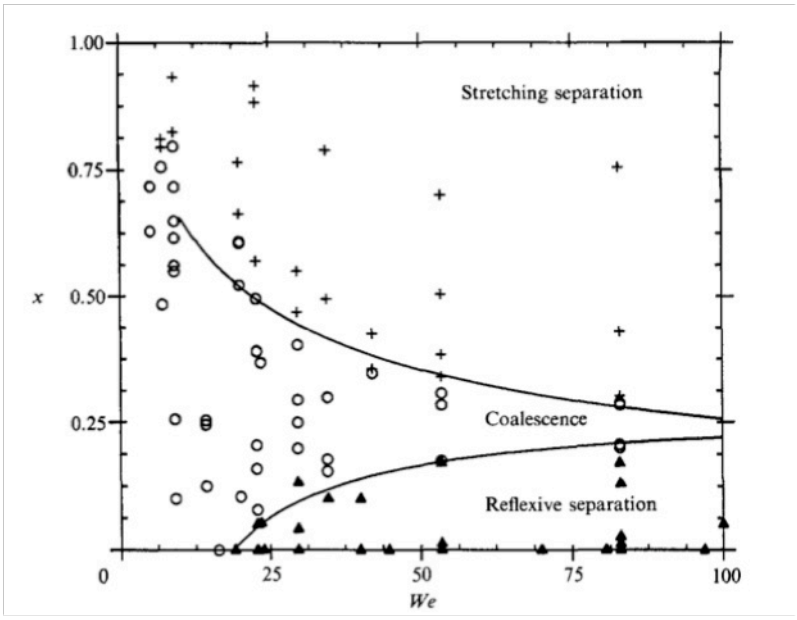

Fig. 2.5: Regions for coalescence and separations(Ashgriz & Poo, 1990).

As one can see from the results, the probability for coalescence after a collision is largest for both low Weber numbers and for low values for the impact parameter.

A closer study on the effects of Reynolds number, impact velocity, drop size ratio and internal circulation on the collision and coalescence process is done by Mashayek, Ashgriz, Minkowycz, & Shotorban (2003).

2.3 Break-up as a Phenomenon

As for collision between particles, break-up occurs in all kinds of multiphase flows. Break-up of bubbles and drops is generally caused by one of the following mechanisms (Dhainaut, 2002):

- Turbulent fluctuations and collisions
- Rayleigh-Taylor and Kelvin-Helmholtz instabilities (which includes rapid acceleration)
- High shear stresses
- Non-uniformity in surfactant distribution

All these mechanisms may lead to local shear forces of the surrounding fluid around the droplet that are greater than the cohesive forces, which is the criterion for break-up to occur.

Droplets can split up in a number of different ways that depend on the flow pattern around them. According to Hinze (1955) there are three basic types of deformation that can lead to break-up: lenticular, cigar-shaped and bulgy. Lenticular deformation is recognized when the droplet is flattened, forming an oblate ellipsoid before it is further deformed into a torus, which breaks into smaller droplets when it is being stretched. Cigar-shaped deformation happens when the droplet is more and more elongated forming a prolate ellipsoid that is further deformed into a long cylindrical thread, which breaks into smaller droplets. Bulgy deformation happens when the surface of the droplet is

deformed locally so bulges occur and parts of the droplet become bodily separated. The three types of deformation are shown in Fig. 2.6.

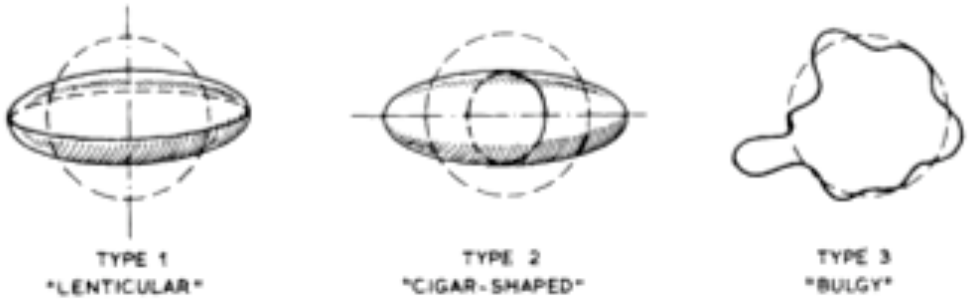

Fig. 2.6: Basic types of droplet deformation (Hinze, 1955).

Also for break-up the dimensionless Weber number is used to characterize the criterion for break-up. For shear flows this dimensionless Weber number is given by:

$$N_{We} = \frac{\rho_c d \overline{v^2}}{\sigma} \tag{2.5}$$

$\overline{v^2}$ is the average of the square of the relative velocity between the particle and the surrounding continuous phase across the flow field. d is the particle diameter, ρ_c is the density of the continuous phase and σ is the surface tension of the system. According to Hinze (1955) the critical value of this number depends on both the viscosity number of the dispersed phase and on how the relative velocity varies with time. The dimensionless viscosity number that characterizes the viscosity of the dispersed phase is given by:

$$N_{Vi} = \frac{\mu_d}{\sqrt{\rho_d \sigma d}} \tag{2.6}$$

Here, μ_d is the viscosity of the dispersed phase. Laboratory experiments and theoretical considerations by Hinze (1955) show that the critical Weber number for break-up to happen, $(N_{We})_{crit}$, increases with increasing N_{Vi}. Indefinitely increase of N_{Vi} leads to $(N_{We})_{crit} \rightarrow \infty$, i.e. no break-up.

For turbulent flows turbulent eddy velocities locally govern the break-up phenomenon. These dynamic pressure forces are caused by changes in the velocity over distances typically of the same order as the particle diameter, i.e. much smaller than the viscous shearing action includes. Break-up occurs when the local shear stress generated by such eddies is larger than surface tension force. The local turbulent shear stress is defined by $1/2\rho_c \overline{u'^2}$, where $\overline{u'^2}$ is the average value of the velocity fluctuations squared. This average value can be related to the particle diameter in order to obtain the critical value, d_{crit}, above which break-up occurs. When using this method, Hinze (1955) found the following relation between d_{crit} and the turbulence energy dissipation rate, ε:

$$d_{crit} \propto \left(\frac{\sigma}{\rho}\right)^{\frac{3}{5}} \varepsilon^{\frac{-2}{5}} \tag{2.7}$$

Only eddies of the same size as the particle can lead to break-up. Smaller eddies do not contain enough energy to break the particle, while larger eddies just move the particle, but are not breaking it up. When break-up occurs, particles may break up into a wide range of sizes.

In the case of hydrodynamic instabilities at the surface of the particle, it may break-up as a consequence of the increasing scroll pattern on the surface. This scroll pattern can exist as one of the two famous hydrodynamic instabilities: the Kelvin-Helmholtz and the Rayleigh-Taylor instability (Fig. 2.7 and Fig. 2.8). The Kelvin-Helmholtz instability occurs when two parallel streams of different velocities that are adjacent to each other become unstable due to perturbations. Rayleigh-Taylor instability occurs when two fluids of different densities interact such that a dense, heavy fluid accelerates a light fluid.

Fig. 2.7: Scroll pattern of the Kelvin-Helmholtz instability (Dhainaut, 2002).

Fig. 2.8: Scroll pattern of the Rayleigh-Taylor instability (Dhainaut, 2002).

3 CFD Modeling of the Continuous Phase

3.1 Introduction to CFD

The purpose of Computational Fluid Dynamics (CFD) is to analyse systems involving fluid dynamics, heat transfer and other associated phenomena by numerical calculations. The areas of application are large and cover both industrial and non-industrial applications.

Generally, a flow can be described by solving the three conservation equations:

- Conservation of mass
- Conservation of momentum
- Conservation of energy

For incompressible flows, the equations for conservation of mass and momentum are referred to as the Navier-Stokes equations. These equations are partial differential equations (PDEs) and thus difficult to solve analytically. A discretization method that approximates the PDEs with a system of algebraic equations is applied and solved numerically on a computer. The algebraic equations are solved for small domains in space and time. The numerical solution of the flow then consists of the solution in these discrete locations. The accuracy of the solution is then dependent on the quality of the discretization method used.

The development of CFD codes has given many advantages in engineering analysis. It is a very useful tool to simulate problems where experiments are very costly. But it should be remarked that CFD simulations are an approximation of real experiments and should not be considered as a substitution for experiments, but rather a complementary.

It exists several CFD codes; most of them are commercial. Among these are CFX, COMSOL and FLUENT. FLUENT is used in the present study.

3.2 Governing Equations for the Continuous Phase

The present work considers particle dispersion and coalescence in a fluid flow. This chapter will state the equations mentioned in the previous chapter used for describing the fluid continuous-phase flow. This study considers water flow with oil droplets in it, which means that only incompressible flow is considered. For incompressible flows the density is constant and not linked to the pressure. The mass conservation is a constraint on the velocity field; this equation (combined with the momentum) can be used to derive an equation for the pressure.

3.2.1 Mass Conservation Equation (Continuity Equation)

The general form of the continuity equation is given by:

$$\frac{\partial \rho}{\partial t} + \nabla \cdot \left(\rho \vec{v} \right) = S_m \tag{3.1}$$

S_m is the mass added to the continuous phase from an eventually dispersed second phase. In the present study this second phase is the liquid oil in water phase. The continuity equation can, for incompressible flows, be simplified to:

$$\nabla \cdot \vec{v} = S_m \tag{3.2}$$

3.2.2 Momentum Conservation Equation

The general form of the momentum conservation is given by:

$$\frac{\partial}{\partial t}\left(\rho\vec{v}\right) + \nabla\left(\rho\vec{v}\vec{v}\right) = -\nabla p + \nabla\cdot\left(\bar{\tau}\right) + \rho\vec{g} + \vec{F} \tag{3.3}$$

$\vec{F}$ is external body forces while $\bar{\tau}$ is the stress tensor:

$$\bar{\tau} = \mu\left[\left(\nabla\vec{v} + \left(\nabla\vec{v}\right)^T\right) - \frac{2}{3}\nabla\cdot\vec{v}I\right] \tag{3.4}$$

3.2.3 Energy Conservation Equation

The general form of the energy conservation equation for incompressible flow can be given as:

$$\frac{\partial T}{\partial t} + \nabla\cdot\left(T\vec{v}\right) = \nabla\cdot\left(\alpha\nabla T\right) + \frac{1}{\rho c_v}\left(\bar{\tau}\cdot\nabla\right)\cdot\vec{v} \tag{3.5}$$

Here, $\alpha = \frac{k}{\rho c_v}$ is the thermal diffusivity. The energy equation (Eq. (3.5)) for incompressible flows is decoupled from the Navier-Stokes equations (Eq. (3.2)-(3.3)). This means that Eq. (3.2)-(3.3) are solved first for $\vec{v}$ and p and then Eq. (3.5) for T.

3.3 Finite-Volume Method

FLUENT uses the Finite-Volume Method (FVM) to discretize and solve the governing equations for the continuous phase. This method consists of three steps:

- Integration of the governing equations over all the control volumes of the domain.
- Discretization and conversion of the resulting integral equations into a system of algebraic equations.
- Solution of the algebraic equations by an iterative method.

In order to get a picture of how the finite-volume method works, a short description of the three steps in the method is given with a general transport equation as an example, cf. (Versteeg & Malalasekera, 1995).

The conservation of a general flow variable ϕ, e.g. a velocity component, within a finite control volume can be expressed as a balance between the various processes tending to increase or decrease it:

$$\begin{bmatrix}\text{Rate of change}\\ \text{of } \phi \text{ in the}\\ \text{control volume}\\ \text{with respect to}\\ \text{time}\end{bmatrix} = -\begin{bmatrix}\text{Net rate of}\\ \text{decrease of } \phi\\ \text{due to convection}\\ \text{into the}\\ \text{control volume}\end{bmatrix} + \begin{bmatrix}\text{Net rate of}\\ \text{increase of } \phi\\ \text{due to diffusion}\\ \text{into the}\\ \text{control volume}\end{bmatrix} + \begin{bmatrix}\text{Net rate of}\\ \text{creation of } \phi\\ \text{inside the}\\ \text{control}\\ \text{volume}\end{bmatrix}$$

The corresponding equation to this expression is given by:

$$\frac{\partial}{\partial t}\left(\rho\phi\right) = -\nabla\cdot\left(\rho\vec{v}\phi\right) + \nabla\cdot\left(\Gamma\cdot\nabla\phi\right) + S_\phi \tag{3.6}$$

Γ is a diffusion coefficient and S_ϕ is a source term. For simplicity the following presentation of the FVM for the general transport equation will be treated as one-dimensional and without source terms (Eq. (3.7)).

$$\frac{\partial}{\partial t}\left(\rho\phi\right) = -\frac{d}{dx}\left(\rho u\phi\right) + \frac{d}{dx}\left(\Gamma\frac{d\phi}{dx}\right) \tag{3.7}$$

This equation can be further simplified by assuming steady state conditions:

$$\frac{d}{dx}\left(\rho u\phi\right) = \frac{d}{dx}\left(\Gamma\frac{d\phi}{dx}\right) \tag{3.8}$$

3.3.1 Spatial Discretization

As mentioned, the principle of the FVM is to discretize the integral form of the governing equations. The integral form of the steady state general transport equation without source terms for an interval [*w*,*e*] in one dimension is given in Eq. (3.9). A sketch of the actual node and its control volume is given in Fig. 3.1.

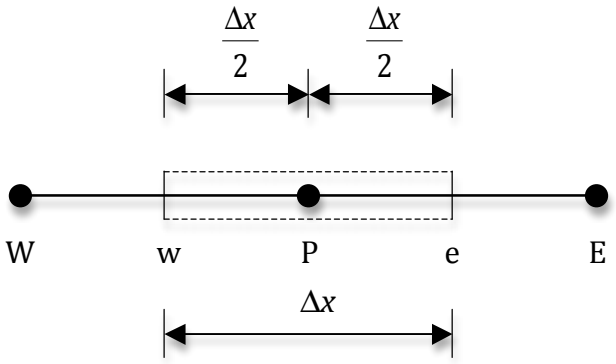

Fig. 3.1: A control volume around node P.

$$\left(\rho uA\phi\right)_e - \left(\rho uA\phi\right)_w = \left(\Gamma A\frac{d\phi}{dx}\right)_e - \left(\Gamma A\frac{d\phi}{dx}\right)_w \tag{3.9}$$

A is the area for the control volume faces; it is assumed to be equal for all faces.

In order to obtain discretized equations for the problem, the terms in Eq. (3.9) must be approximated. By introducing two new variables *F* and *D*, as given in Eq. (3.10), the approximated transport equation can be written as in Eq. (3.11).

$$\begin{aligned} F &= \left(\rho u\right), \quad D = \frac{\Gamma}{\Delta x} \\ F_w &= \left(\rho u\right)_w, \quad D_w = \frac{2\Gamma_w}{\Delta x} \\ F_e &= \left(\rho u\right)_e, \quad D_e = \frac{2\Gamma_e}{\Delta x} \end{aligned} \tag{3.10}$$

$$F_e\phi_e - F_w\phi_w = D_e\left(\phi_E - \phi_P\right) - D_w\left(\phi_P - \phi_W\right) \tag{3.11}$$

The next step is to approximate the face values ϕ_e and ϕ_w. There exist several methods for spatial discretization. (Fluent Inc., 2006) presents a short description of some of the schemes for this discretization:

- *First-Order Upwind Scheme:*
  Upwinding means that the cell-face value of the current cell is derived from the quantities of the cell upstream or "upwind" relative to the direction of the normal velocity. For the first-order upwind method the cell-center value of a cell is assumed to represent a cell-average value for the cell. Thus, the face value of the current cell is set equal to the cell-center value of the upstream cell:
  $$\phi_e = \phi_p \text{ and } \phi_w = \phi_W \tag{3.12}$$

- *Second-Order Upwind Scheme:*
  Second-order accuracy is achieved at cell faces through a Taylor series expansion of the cell-centered solution about the cell centroid. Thus the face value of the current cell, ϕ, is computed by:
  $$\phi_e = \phi_p + \left(\nabla\phi\right)_p \cdot \vec{r} \text{ and } \phi_w = \phi_W + \left(\nabla\phi\right)_W \cdot \vec{r} \tag{3.13}$$

  ϕ and $\nabla\phi$ are the cell-centered value and its gradient in the upstream cell, while $\vec{r}$ is the displacement vector from the upstream cell centroid to the face centroid.

Generally the accuracy will be improved by choosing a higher-order scheme because the first-order scheme has a numerical diffusivity because of its numerical dissipation term (Müller, 2007). But as the order of the scheme is increased, convergence is more difficult to achieve. When the flow is aligned with the grid, the first-order upwind scheme may be acceptable. In other words, for triangular and tetrahedral grids it is generally more accurate results with higher-order schemes, since the flow is never aligned with the grid. But for quadrilateral schemes the results may be acceptable.

3.3.2 Temporal Discretization

For transient problems, like the general transport equation problem, the governing equations must be discretized not just in space, but also in time. Every term in the equations must be integrated over a time step Δt, from time level n to n+1. By writing the transport equation as Eq. (3.14), the time integration can be done like in ordinary differential equations, as shown in Eq. (3.15).

$$\frac{\partial(\rho\phi)}{\partial t} = -\frac{d}{dx}(\rho u\phi) + \frac{d}{dx}\left(\Gamma\frac{d\phi}{dx}\right) = f\left(t,\phi(t)\right) \tag{3.14}$$

$$\int_{t_n}^{t_{n+1}} \frac{\partial(\rho\phi)}{\partial t} dt = \int_{t_n}^{t_{n+1}} f\left(t,\phi(t)\right) dt \tag{3.15}$$

As for the spatial discretization there exist several schemes for temporal discretization. (Fluent Inc., 2006) gives a short description of some of these schemes (incompressible flow is assumed, ρ = const.):

- *First-Order Implicit Scheme:*
  In the implicit method the function $f(t,\phi(t))$ is evaluated at the future time level. It is called "implicit" because ϕ^{n+1} in a given cell is related to ϕ^{n+1} in the neighboring cell through $f(t,\phi(t))$. This means that the equation must be solved iteratively at each time level before moving to the next time step. The resulting FVM for the transport equation can then be written as:
  $$\frac{\rho\left(\phi^{n+1}-\phi^{n}\right)}{\Delta t} = f\left(t_{n+1},\phi^{n+1}\right) \tag{3.16}$$

- *Second-Order Implicit Scheme:*
  Second order accuracy is achieved by choosing a more accurate finite difference stencil for the approximation of the temporal derivative. The resulting FVM then becomes:
  $$\frac{\rho\left(3\phi^{n+1}-4\phi^{n}+\phi^{n+1}\right)}{2\Delta t} = f\left(t_{n+1},\phi^{n+1}\right) \tag{3.17}$$

- *Explicit Scheme:*
  The explicit method evaluates $f(t,\phi(t))$ at the current time level. It is referred to as "explicit" because ϕ^{n+1} can be expressed explicitly in terms of known values, ϕ^{n}. The explicit method provided in FLUENT is first-order accurate. The resulting FVM for this method is given by:
  $$\frac{\rho\left(\phi^{n+1}-\phi^{n}\right)}{\Delta t} = f\left(t_{n},\phi^{n}\right) \tag{3.18}$$

3.3.3 Assembly of the Discretized Equations

When the governing equations are discretized with one of the schemes described above, the discretized equations must be assembled to a matrix system of algebraic equations. This matrix system can be solved by several different techniques; however, the most popular solution procedure is by the TDMA (tri-diagonal matrix algorithm) line-by-line solver (Versteeg & Malalasekera, 1995). Equation (3.19) and (3.20) shows the algebraic equation for the one-dimensional general transport equation without source term at each control volume, while Eq. (3.21) shows the form of the resulting matrix system that is obtained by combining these equations for all control volumes.

$$a_W \phi_W + a_P \phi_P + a_E \phi_E = a_P^0 \phi_P^0 \tag{3.19}$$

$$a_P \phi_P + \sum_{nb} a_{nb} \phi_{nb} = a_P^0 \phi_P^0 \tag{3.20}$$

$$\left[A\right] \cdot \left[\phi\right] = \left[B\right] \tag{3.21}$$

In Eq. (3.21) the term [B] contains the initial values, $a_P{}^0 \phi_P{}^0$, and boundary conditions. See (Versteeg & Malalasekera, 1995) for details about how the coefficients in the algebraic equations vary when different discretization schemes are used, and how boundary conditions enter the discretization and assembly of the governing equations.

3.4 Algorithm for Pressure-Based Calculations

The present study does not include the energy equation in the calculations because no heat transfer in assumed (c.f. Chapter 5.2). Thus, some special practices related to the discretization of the continuity and momentum equations when the solver is pressure-based (segregated) are discussed in this chapter.

The momentum equations and the continuity equation are coupled because every velocity component appears in all equations. But the most complex issue to resolve is the pressure field since it appears in all momentum equations. There is no equation for that resolves the pressure. If the pressure gradient is known, the discretized equations for velocity are obtained in exactly the same manner as for any other scalar. But for most flow computations, also the one in this study, it is desirable to calculate the pressure field as part of the solution, hence the pressure gradient is normally not known beforehand. If the flow is incompressible, as it is assumed to be in this study, the density is constant and do not depend on the pressure. The coupling between the pressure and velocity thus implies that if the correct pressure field is applied in the momentum equations the resulting velocity field should satisfy continuity.

The schemes presented for discretization of the general transport equations in Chapter 3.3 is also used to discretize the momentum equations in the pressure-based solution algorithm. The steady state x-momentum equation without source terms can be obtained by setting ϕ=u:

$$a_P u = \sum_{nb} a_{nb} u_{nb} + \sum p_f A_{fx} \tag{3.22}$$

Equation (3.22) requires the value of the pressure at the face between cells c_0 and c_1, as shown in Fig. 3.2. Thus, an interpolation scheme is necessary to calculate this value. A standard scheme is chosen in the present study. See (Fluent Inc., 2006) for details about this scheme. FLUENT uses a co-located scheme where pressure and velocity are stored at cell centers.

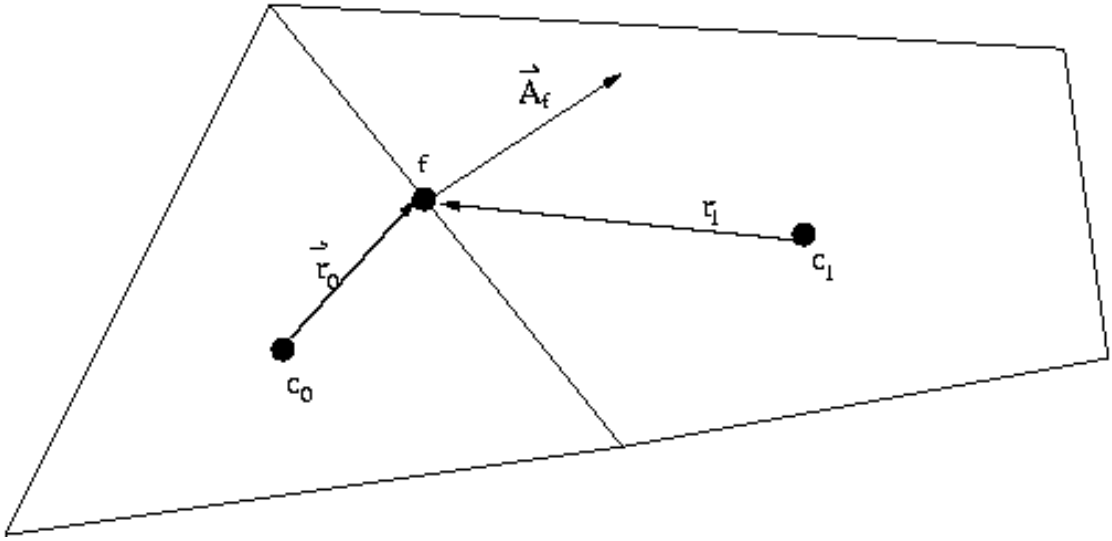

Fig. 3.2: Control volume with discretization parameters (Fluent Inc., 2006).

By integrating the continuity equation over the control volume in Fig. 3.2 the following discrete equation is obtained:

$$\sum_{f}^{N_{faces}} J_f A_f = 0 \tag{3.23}$$

J_f is the mass flux through face *f*.

The problem with pressure-velocity linkage can be resolved by adopting an iterative solution strategy. The strategy used in this study, and also one of the most common strategies, is the SIMPLE (Semi-Implicit Method for Pressure Linked Equations) algorithm. The principle of the algorithm is that a guessed pressure field, p^*, is used to solve the discretized momentum equations and then enforce the mass conservation and obtain the pressure field. As the next step, the corrections of the pressure and mass flux, p' and J_f', are defined as the difference between the correct and guessed pressure and mass flux, respectively:

$$\begin{aligned} p &= p^* + p' \\ J_f &= J_f{}^* + J_f{}' \end{aligned} \tag{3.24}$$

The SIMPLE algorithm does the following approximation:

$$J_f{}' = d_f \left(p_{c_0}{}' - p_{c_1}{}' \right) \tag{3.25}$$

Here, $d_f = \frac{A_f}{a_p}$.

A discrete equation for the pressure correction, p', in the cell is then obtained by substituting the flux correction equation into the discrete continuity equation, Eq. (3.23):

$$a_p p' = \sum_{nb} a_{nb} p_{nb}' \tag{3.26}$$

Once the solution for the correction pressure is calculated, the cell pressure and the face flux are corrected using the following relations:

$$p = p^* + \alpha_p p' \tag{3.27}$$

$$J_f = J_f^* + d_f \left(p_{c_0}' - p_{c_1}' \right) \tag{3.28}$$

Here, α_p is the under-relaxation factor for pressure. See (Versteeg & Malalasekera, 1995) for details about the use of under-relaxation. This iterative process is repeated until convergence of the corrected values.

3.5 Turbulence Modeling

All flows encountered in engineering practice become unstable above a certain Reynolds number. Turbulence is caused by the development of a chaotic and random state of motion in which the velocity and pressure change continuously with time within regions of flow. Most flows of engineering significance are turbulent, so the turbulence flow regime is of great interest in the engineering industry. The present study does also contain turbulent flows, hence turbulence modeling is thus needed.

One of the most difficult hurdles to the proper use of CFD codes is the turbulence modeling. In a turbulent flow, particles of fluid move unsteadily in an unpredictable path. In most CFD codes different turbulence models are proposed. Turbulent flows are characterized by fluctuating velocity fields. These fluctuations can be of small scale and high frequency and then become too computational time consuming when simulated in engineering calculations.

Turbulence modeling is based on the principle that the velocity can be decomposed into a steady mean value and a fluctuating component of the velocity. This is called the Reynolds decomposition. The turbulent flow is then characterized in terms of the mean values of flow properties and some statistical properties of their fluctuations. By implementing this characterization into the momentum equations for the flow the Reynolds-Averaged Navier-Stokes (RANS) equations can be derived. In order to be able to compute turbulent flows with the RANS equations it is necessary to develop turbulence models to predict the Reynolds stresses and the scalar transport terms and close the system of mean flow equations. The number of additional transport equations needed along with

the RANS equations in order to close the system classifies the most common RANS turbulence models.

The different turbulence models have different pros and cons. Since the Reynolds-Stress Equation Model (RSM) accounts for the effects of streamline curvature, swirl, rotation, and rapid changes in strain rate in a more rigorous manner than one-equation and two-equation models, it has greater potential to give accurate predictions for complex flows, such as the rotating low in the present study. Thus, this model is chosen as the turbulence model, even though it is a seven-equation model for three-dimensional problems (five-equation model for two-dimensional problems) and needs more computational power and time to be solved.

3.5.1 Transport Equations for the Reynolds-Stress Equation Model

Taking moments of the exact momentum equation derives the exact form of the Reynolds stress transport equations. This is a process wherein the exact momentum equations are multiplied by a fluctuating property, the product then being Reynolds-averaged. Unfortunately, several of the terms in the exact equation are unknown and modeling assumptions are required in order to close the equations.

The exact equation for the transport of kinematic Reynolds stress, $R_{ij} = \overline{u_i' u_j'}$, takes the form given in Eq. (3.29) (Versteeg & Malalasekera, 1995).

$$\underbrace{\frac{\partial R_{ij}}{\partial t}}_{\text{Rate of change}} + \underbrace{C_{ij}}_{\text{Convection}} = \underbrace{P_{ij}}_{\text{Production}} + \underbrace{D_{ij}}_{\text{Diffusion}} - \underbrace{\varepsilon_{ij}}_{\text{Dissipation}} + \underbrace{\Pi_{ij}}_{\text{Pressure strain}} + \underbrace{\Omega_{ij}}_{\text{Rotation}} \tag{3.29}$$

The six terms in Eq. (3.29) are modeled by six different equations for the Reynolds stress transport. Along with these, a model equation for the scalar dissipation rate, ε, is solved. This makes the Reynolds-Stress Equation Model contain seven equations, which have to be solved along with the exact equation for transport of kinematic Reynolds stress. More details about the development and use of this model can be found in (Versteeg & Malalasekera, 1995).

3.6 General Procedure for Use of CFD codes

CFD-codes are all structured around the numerical algorithm that will solve the fluid flow problems. The CFD code consists of three fundamental elements:

- Pre-processor
- Solver
- Post-processor

3.6.1 Pre-processor

The task of the pre-processor, i.e. GAMBIT, is to gather the essential information, the inputs, needed to solve the flow problem. This involves the following steps:

- Definition of the geometry, i.e. the computational domain, by creating volumes, surfaces, edges and points.

- Generation of the grid, i.e. sub-division of the computational domain into smaller sub-domains. Meshes can be both triangular and quadrilateral.
- Specification of boundaries and continuum zone types.

3.6.2 Solver

Once the mesh is created it is saved as a binary file, which can be read by the solver. When the file is read in the solver, the first thing to do is to make sure that all the volumes created are positive. The user defines models for solver, energy, viscosity, turbulence and radiation. Initial- and boundary conditions need to be specified, as well as properties of the different fluids present in the system. Different schemes for both temporal and spatial discretization are available as described in Chapter 3.3. The user selects the desired level of convergence. Before the iteration process can start, it is necessary to initialize the entire flow field, such as ambient pressure, velocity and temperature. By using different zones in the flow field it is possible to make different initial conditions for different parts of the flow field. The flow calculations can be based on different numerical solution techniques, but the finite volume method is the most common technique when it comes to fluid flow calculations. The finite-volume technique is used in the CFD code FLUENT used in the present study. To check the convergence of the solution FLUENT uses residuals. The residual for continuity, velocity components, and variables related to the chosen turbulence model is calculated in each iteration step. The residual for each variable is the difference between the value calculated at iteration N-1 and iteration N divided by its physical time step. The convergence criterion can be decreased to obtain more accurate results but it also increases dramatically the CPU time.

3.6.3 Post-processor

Once the solution has converged, the post-processor provides plotting and animation of contours and vectors, tracking of particles in the flow and several other visualization tools. Most CFD packages, such as FLUENT, are equipped with such tools.

4 Dispersed Phase Modeling: Coalescence and Break-up

4.1 Eulerian and Lagrangian Framework

When multiphase flow problems are to be solved, there are mainly two different classes of approaches that could be used for modeling of the dispersed phase: the Eulerian and the Lagrangian modeling. In the Eulerian approach the dispersed phase is treated as a continuum that interacts with the continuous phase, while in the Langrangian approach the trajectory of each parcel in dispersed phase is found by solving the Lagrangian equations of mass and momentum. Both the coalescence and break-up phenomenon can be modeled with both of the two above approaches. There are several possibilities of methods for modeling these phenomena in both the Eulerian and Langrangian framework. The majority of the investigations have been looking at these phenomena separately. Thus, many models that contain only one of these phenomena are made, but some models that combine both phenomena has been made; most of these are based on the theory of population balances (Ramkrishna, 2000). This approach is based on a differential equation that accounts for birth and death of particles within the flow field. The equation has to be coupled with a Eulerian approach for solving the dispersed phase. The present work will investigate turbulence dispersion and the coalescence and break-up phenomena using a Langrangian approach. In FLUENT, the method available for Langrangian modeling of the dispersed phase is the discrete phase model (DPM). A further description of this model and the model's handling of coalescence and break-up are given in the following sections.

4.2 Discrete Phase Model (DPM)

The discrete phase model in FLUENT provides the possibility to simulate, in addition to the transport equations for the continuous phase, a discrete second phase in a Lagrangian frame of reference. The second phase consists of spherical particles that are intended to represents drops or bubbles dispersed in the continuous phase.

This means that the discrete phase model follows an Euler-Lagrange approach. The fluid (continuous) phase is solved by the time-averaged Navier-Stokes equations, while tracking of all particles, bubbles or droplets through the calculated flow field solves the dispersed phase. This phase exchanges momentum and eventually heat and mass with the fluid phase.

(Fluent Inc., 2006) mentions some limitations of the model. Since the particles are tracked individually (one by one), the computational time may be very large. Thus, a very important assumption made for this model is that the dispersed phase occupies a low volume fraction, usually less than 10-12%. This is because the model assumes that particle-particle interactions and the effects of the particle volume fraction on the fluid phase are negligible. Another limitation is that the steady-particle Lagrangian discrete phase model is only suited for flows in which particle streams are injected into a fluid phase flow with a well-defined entrance and exit condition. However, the unsteady-particle discrete phase

model is capable of modeling continuous suspension of particles. See (Fluent Inc., 2006) for limitations on using the discrete phase model with other FLUENT models.

The particle motion is determined by integrating the force balance of the particle. This force balance says that the particle's inertia is equal to the forces acting on the particle. For the x-direction in Cartesian coordinates this is given by:

$$\frac{du_p}{dt} = F_D\left(u - u_p\right) + \frac{g_x\left(\rho_p - \rho\right)}{\rho_p} + F_x \tag{4.1}$$

F_x is an additional acceleration term, $F_D(u\text{-}u_p)$ is the drag force per unit particle mass. F_D is given from:

$$F_D = \frac{18\mu}{\rho_p d_p^2}\frac{C_D \mathrm{Re}_{rel}}{24} \tag{4.2}$$

The drag coefficient, C_D, may be taken from different relations. Morsi & Alexander (1972) (Eq. (4.3)) and Haider & Levenspiel (1989) (Eq. (4.4)) provide two different relations for the drag coefficient and details about the factors included in the relations.

$$C_D = a_1 + \frac{a_2}{\mathrm{Re}_{rel}} + \frac{a_3}{\mathrm{Re}_{rel}^2} \tag{4.3}$$

$$C_D = \frac{24}{\mathrm{Re}_{rel}}\left(1 + b_1 \mathrm{Re}_{rel}^{b_2}\right) + \frac{b_3 \mathrm{Re}_{rel}}{b_4 + \mathrm{Re}_{rel}} \tag{4.4}$$

In the above equations, u is the fluid phase velocity, u_p is the particle velocity, μ is the molecular viscosity of the fluid, ρ is the fluid density, ρ_p is the density of the particle, and d_p is the particle diameter. Re_{rel} is the relative Reynolds number, defined by:

$$\mathrm{Re}_{rel} \equiv \frac{\rho d_p \left|u_p - u\right|}{\mu} \tag{4.5}$$

Equation (4.1) includes additional forces, called F_x. These are important under certain circumstances. Among these are the "virtual mass" force, the force required to accelerate the fluid surrounding the particle. Another is the additional force that exists because of pressure gradient in the fluid. Both forces are important when $\rho > \rho_p$, and are given in Eq. (4.6)-(4.7), respectively.

$$F_x = \frac{1}{2}\frac{\rho}{\rho_p}\frac{d}{dt}\left(u - u_p\right) \tag{4.6}$$

$$F_x = \left(\frac{\rho}{\rho_p}\right) u_{p_i} \frac{\partial u}{\partial x_i} \tag{4.7}$$

A thermophoretic force may also be included in the additional force term in Eq. (4.1). This phenomenon is when small particles suspended in a gas that has a temperature gradient experience a force in the direction opposite to that of the gradient. See (Fluent Inc., 2006) for details on this force.

The dispersion of particles in the fluid phase due to turbulence can be modeled in two ways: stochastic tracking or particle cloud tracking. The stochastic tracking model uses stochastic methods to predict the effect of instantaneous velocity fluctuations on the particle trajectories. The particle cloud model tracks a statistical evolution of a cloud of particles about a mean trajectory. See(Fluent Inc., 2006) for details on the turbulent dispersion of particles.

Equation (4.1) must be discretized in order to be able to solve the equation numerically. Before doing that, it is convenient to put the equation into the following general equation set:

$$\frac{dx}{dt} = u_p \tag{4.8}$$

$$\frac{du_p}{dt} = \frac{1}{\tau_p}\left(u - u_p\right) + a \tag{4.9}$$

The term *a* includes accelerations due to all other forces than the drag force. Several discretization schemes for solving Eq. (4.9) are available in FLUENT. The present study has used trapezoidal tracking as the high-order scheme and implicit discretization as the low-order scheme. Trapezoidal discetization of Eq. (4.9) gives:

$$u_p^{n+1} = \frac{u_p^n\left(1 - \frac{1}{2}\frac{\Delta t}{\tau_p}\right) + \frac{\Delta t}{\tau_p}\left(u^n + \frac{1}{2}\Delta t u_p^n \cdot \nabla u^n\right) + \Delta t a}{1 + \frac{1}{2}\frac{\Delta t}{\tau_p}} \tag{4.10}$$

For the implicit scheme, the discretization of Eq. (4.9) gives:

$$u_p^{n+1} = u_p^n + \frac{\Delta t\left(a + \frac{u^{n+1} - u_p^{n+1}}{\tau_p}\right)}{1 + \frac{\Delta t}{\tau_p}} \tag{4.11}$$

For both schemes the new particle location is computed by an explicit trapezoidal discretization of Eq. (4.8):

$$x_p^{n+1} = x_p^n + \frac{1}{2}\Delta t\left(u_p^n + u_p^{n+1}\right) \tag{4.12}$$

4.3 Coalescence Modeling

Equation (4.1)-(4.7) describe the particle motion only. The discrete phase model does also include simulation of what happens when particles collide, both the number of collisions and their outcomes in a computationally manner. If the collisions and their outcomes should be calculated for each possible collision pair the computational cost would be prohibitive. Thus, a model that reduces the number of calculation is needed. O'Rourke (1981) made an algorithm that efficiently reduces the computational cost of these calculations. This algorithm has been commonly used in many commercial applications for numerical simulation of the droplet collision process, also in the discrete phase model in FLUENT. The method is a stochastic estimate of collisions. Parcels, which are statistical representations of a number of individual droplets, are used to describe the collisions instead of particles. The equation about the collision probability is derived using classical kinetic theory on the basis of the assumption that the particles were uniformly distributed in the spray of particles and the droplet collision had similarity to the molecular collision process. Another assumption is that two parcels may collide only if they are located in the same continuous-phase cell. The model does also include post-characteristics of droplets using the balance equations of mass, momentum and energy between before and after collision.

In order to derive the probability of collision O'Rourke (1981) uses the relative distance and relative velocity between the two colliding droplets. He defined the collision cross section as the circle centered on the larger droplet's center that the smaller droplet's center has to pass within so that collision takes place:

$$\sigma_{l,s} = \pi\left(r_l + r_s\right)^2 \tag{4.13}$$

The indexes *l* and *s* represent the larger and smaller drop respectively, and *r* represents the radius of a droplet. The collision volume is then the collision cross section multiplied by the distance traveled by the relative velocity:

$$V_{col} = \sigma_{l,s} u_{rel} \Delta t \tag{4.14}$$

O'Rourke's algorithm then determines the collision probability by calculating the probability of the smaller droplet being in the collision volume. Since the probability of the droplet being anywhere in the continuous-phase cell of volume *V* is uniform within the cell, the probability of the smaller droplet colliding with the larger is equal to the ratio between the two volumes:

$$P_{l,s} = \frac{V_{col}}{V} \tag{4.15}$$

Thus, the mean expected number of collisions between a droplet in parcel *l* and the droplets in parcel *s* is given by:

$$\overline{n} = \frac{n_s V_{col}}{V} \tag{4.16}$$

The number of droplets in parcel s is n_s. The actual number of collisions is determined by sampling from a Poisson distribution:

$$P(n) = e^{-\bar{n}} \frac{\bar{n}^n}{n!} \tag{4.17}$$

Here, n is the number of collisions between two droplets.

Once a collision has occurred, the collision outcome must be determined. (O'Rourke, 1981) considers three types of outcomes; bouncing, coalescence and separation, but it ignores the formation of satellite droplets. The boundaries between the regimes adopted in the model for equal-sized droplets are shown in Fig. 4.1.

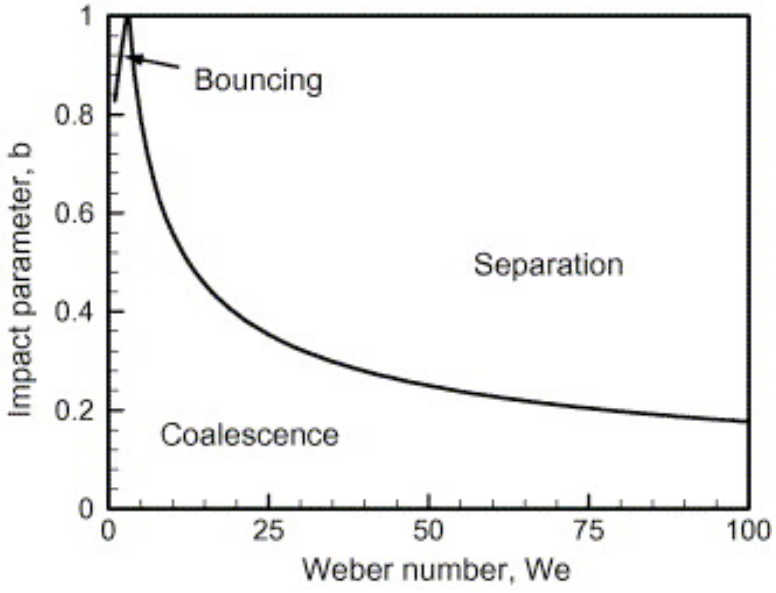

Fig. 4.1: Boundaries between collision regimes (Ko & Ryou, 2005).

The criterion for coalescence is related to the coalescence collision frequency, given by:

$$E_{coal} = \min\left[1, \frac{24 f(\gamma)}{We}\right] \tag{4.18}$$

The function $f(\gamma)$ can be found from:

$$f(\gamma) = \gamma^3 - 2.4\gamma^2 + 2.7\gamma \tag{4.19}$$

Here, γ is the drop size ratio:

$$\gamma = \frac{d_l}{d_s} = \frac{1}{\Delta} \tag{4.20}$$

Coalescence occurs if the impact parameter x in Eq. (2.3) is less than E_{coal}. Otherwise separation will occur. The impact parameter squared is chosen to be a

random number from a uniform distribution in the range [0,1]. This can be done because in a turbulent spray all values of the impact parameter squared are equally likely.

The post-collision properties of the coalesced droplets are found from the basic conservation equations of mass, linear momentum and angular momentum. In the separation and grazing bounce regimes the new velocities are calculated based on conservation of momentum and kinetic energy, no mass is assumed to exchange between two colliding droplet parcels. The new velocities are given by:

$$u_{s,l} = \frac{\rho_{s,l} d_{s,l}^3 u_{s,l} + \rho_{l,s} d_{l,s}^3 u_{l,s} + \rho_{l,s} d_{l,s}^3 \left(u_{s,l} - u_{l,s}\right)}{\rho_{s,l} d_{s,l}^3 + \rho_{l,s} d_{l,s}^3} \left(\frac{x - \sqrt{E_{coal}}}{1 - \sqrt{E_{coal}}} \right) \tag{4.21}$$

4.4 Break-up Modeling

The discrete phase model does include two different models for describing the break-up process: the Taylor analogy break-up (TAB) model for describing low – Weber-number flows, and the wave model for higher-Weber-number flows (Weber number greater than 100). The TAB model is used in the present study since high-speed flows are not studied; none of the simulated cases involve average Weber number higher than approximately 1.3.

The TAB model is based upon Taylor's analogy between an oscillating and distorting droplet and a spring mass system. The surface tension forces is equivalent to the restoring force of the spring, the droplets drag force is represented by the external force of the spring-mass system, while the droplet viscosity forces is analogous to the damping force of the spring-mass system. The principle of the method is further that when the droplet oscillations grow to a critical value the "mother" droplet breaks into several smaller "child" droplets.

The equations governing a damped forced oscillator is:

$$F_{Taylor} - k_{Taylor} x - d_{Taylor} \frac{dx}{dt} = m \frac{d^2 x}{dt^2} \tag{4.22}$$

Here, x is the displacement of the droplets equator from its undisturbed position. By using Taylor's analogy, which describes the coefficients, and putting Eq. (4.22) in nondimensionalized form ($y = \frac{x}{C_b r}$), one obtains:

$$\frac{d^2 y}{dt^2} = \frac{C_F}{C_b} \frac{\rho_c}{\rho_d} \frac{u_{rel,phases}^2}{r^2} - \frac{C_k \sigma}{\rho_d r^3} y - \frac{C_d \mu_d}{\rho_d r^2} \frac{dy}{dt} \tag{4.23}$$

Here, r is the droplet radius, C_F, C_k, C_d, and C_b are constants, σ is the surface tension, and ρ_c and ρ_d are the density of the continuous and the dispersed phase, respectively.

To determine whether or not the droplet breaks up, the amplitude for an undamped oscillation for each droplet at time step *n* is used:

$$A = \sqrt{\left(y^n - We_{crit}\right)^2 + \left(\frac{\left(dy/dt\right)^n}{\omega}\right)^2} \tag{4.24}$$

Break-up is only possible if the following condition is satisfied:

$$We_{crit} + A > 1 \tag{4.25}$$

The following relation gives We_{crit}:

$$We_{crit} = \frac{C_F \rho_c u_{rel,phases}^2 r}{C_k C_b \sigma} \tag{4.26}$$

The next time step must also be calculated to find the value of *y* and its derivative at the next time level. Using a discretized form of the integrated form of Eq. (4.23) does this. The size of the child droplets is determined from the assumption that the energy of the parent droplet equals the combined energy of the child droplets, and the number of child droplets is determined by mass conservation (Fluent Inc., 2006).

4.5 Coupling Between the Phases

When modeling dispersed phase problems, the most important things to consider are the forces acting on the dispersed phase due to the effect of the motion of the continuous phase. When only this effect is considered the approach is called one-way coupling. When taking into account that also the continuous phase flow pattern is impacted by the dispersed phase the approach is called two-way coupling. In denser flows with larger volume fraction of particles, the effects of particle-particle interaction and turbulent modulation (effects of the dispersed phase on the continuous phase turbulent eddies) become more prevailing and should be included in the modeling. When these phenomena are also included, the approach is called four-way coupling. The need for these three approaches is shown in Fig. 4.2. For very dilute flows (volume fraction<10^{-6}) the effects of the dispersed phase on the continuous phase are negligible. Larger volume fractions (<10^{-3}) imply that two-way coupling is necessary. Even larger fractions (>10^{-3}) require all effects between the two phases to be taken into account and four-way coupling should be used.

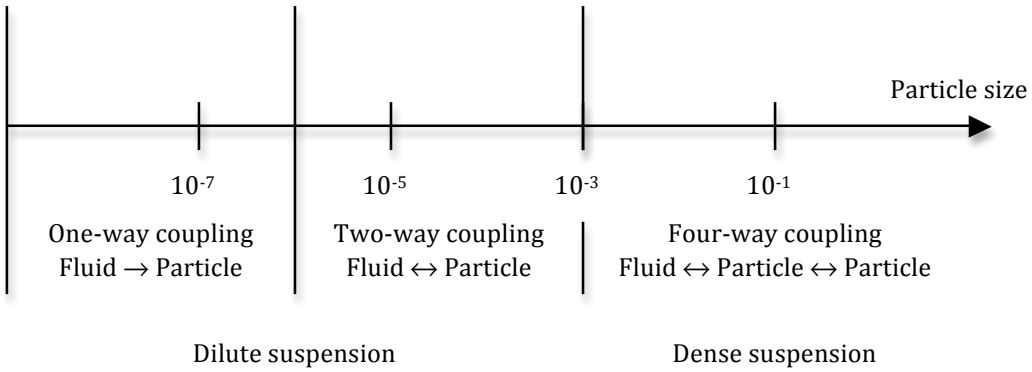

Fig. 4.2: Map of flow regimes.

The discrete phase model in FLUENT does not include a fully four-way coupled solution algorithm, it does not account for turbulent modulation, but it contains a two-way coupled algorithm. Alternately solving the dispersed and continuous phase equations accomplish this two-way coupling until the solutions in both phases have stopped changing.

The present study does not consider heating/cooling, evaporation, boiling or surface reactions, hence only momentum exchange between the two phases is considered. Thus, only exchange of momentum between the phases is included in the model. This term is computed as the change in momentum of a particle as it passes through each control volume:

$$F = \sum \left(\frac{18\mu C_D \mathrm{Re}}{\rho_d d_p^2 24} \left(u_p - u \right) + F_{other} \right) \dot{m}_p \, \Delta t \tag{4.27}$$

5 Methodology and Simulation Set-up

5.1 Physical Description of the Problem

As mentioned in the introduction, the principle of the Compact Tubular Coalescer (CTC) is to force the flow consisting of water with oil droplets into a controlled turbulent and centrifugal flow pattern. The aim is to get the oil droplets to migrate into the middle of the tube and coalesce so the average diameter increases. The larger droplets can then more easily be removed from the water flow. This is done by a swirl element, which is inserted into a cylinder formed pipe. This swirl element is presented in Fig. 5.1. The CTC does not consist of any moving or rotating parts, which makes it compact and easy to use and implement among other processing equipment. A description of how the model of the CTC is made in this study and the computational conditions is presented in the following sections.

Fig. 5.1: Swirl element.

5.2 General Assumptions for the Model of the CTC

In order to achieve the desired operating conditions for the simulations, several assumptions have to be made for the model. These have to be given as inputs in FLUENT. The following general assumptions concerns all investigations done in the present study:

- Gravitation is included; the gravitational acceleration is set to 9.81 m/s^2 in the negative y-direction, which means straight downward.

- All walls are treated as aluminum walls and considered adiabatic, which means that heat transfer between walls and fluid are neglected.

- The boundary condition at the inlet of the CTC is constant velocity of 2 m/s, while the pressure is held constant at the outlet, equal to the operating pressure (1 atm = 101325 Pa).

- The continuous phase flow is considered to be turbulent. This means that a turbulence model must be chosen; the Reynolds-Stress Equation Model is chosen because of its capability to account for effects of streamline

curvature and swirl, which is essential when modeling the swirling flow in the CTC. See Chapter 3.5 for details about the RSM turbulence model.

- The fluid used for the continuous phase is liquid water. The properties for water is taken from FLUENT's library of fluid properties. The density is set to be constant since water may be considered as approximately incompressible. A commonly accepted limit for a flow to be considered as incompressible is (White, 2003):

$$Ma = \frac{u}{c} \leq 0.3 \tag{5.1}$$

- The oil droplets are in most cases modeled as liquid diesel, which has similar properties to e.g. hydrate. They are injected from the inlet area of the CTC. See Chapter 5.4 for details about the impact of the different investigations. The properties of these liquids are also taken from FLUENT's library.

- The diameter distribution at the inlet of the CTC is assumed to be uniform, i.e. all droplets entering the computational domain have the same initial diameter.

- In the break-up modeling it is assumed that a droplet can only break up into two child droplets.

- It is assumed that no heat and mass transfer between the dispersed and continuous phase occur. Only momentum exchange is considered.

- The problem is modeled as three-dimensional, thus the 3D version of FLUENT 6.3.26 is run.

All simulations of the present work are done on a computer with an Intel Core Duo CPU with a capacity of 2.2 GHz. All settings used for simulation of the water phase in FLUENT are summarized and presented in Table B.1. Settings for solution controls are presented in Table B.2.

5.3 Set-up of the CTC Model

5.3.1 General Description of the CTC Model

Because of the complexity of the flow with both turbulence and swirling flow, the CTC is modeled as three-dimensional. The geometry for the model is made to simulate in the best possible way what will happen in a real physical CTC. The geometry is quite simple. It consists of a cylinder in which a swirl element is inserted (Fig. 5.1). The cross sectional area of the CTC is shown in Fig. 5.2. Both the outer wall and the swirl element are considered as aluminum walls, while the inlet velocity and the outlet pressure are held constant.

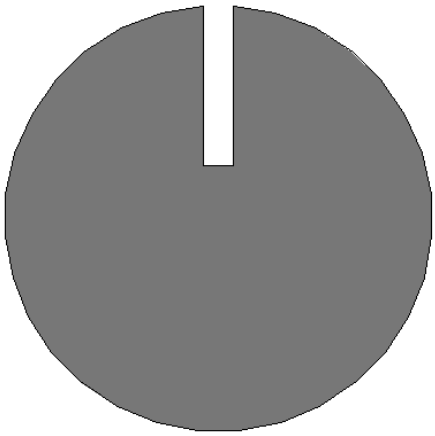

Fig. 5.2: Illustration of the cross-sectional area of the CTC.

5.3.2 Discretization of the Model

The grid is created in GAMBIT. The volume is meshed by means of a TGrid meshing scheme. This means that the mesh primarily consists of tetrahedral mesh elements, but hexahedral, pyramidal, and wedge elements may be included where appropriate. The grid is made with an equal distance of 0.0035 m between each node. The grid consisted of 176205 cells in total. The length is 1 m and the diameter is 4 cm. The swirl element consists of 12 loops. See Chapter 6.1.1 for details of how the grid size is chosen. The grid is presented in Fig. 5.3.

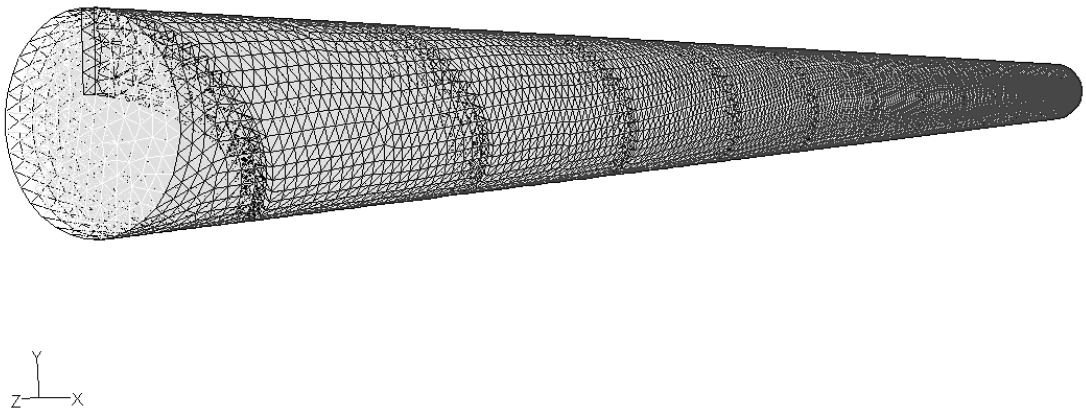

Fig. 5.3: Grid created for the CTC.

5.4 How the Simulations are Carried Out

The simulations are carried out during three steps. The first step was to initialize the flow field. This was done with the settings defined for the boundary conditions at the inlet. No particle injection is done in this step. The second step was to run this simulation stationary until convergence was reached. This was done by first reaching convergence with a first-order upwind spatial discretization method for the momentum and turbulence equations, and then switching to a second-order upwind method to achieve a fully converged solution of the flow field. The default values for the under-relaxation factors are chosen. The third step was to define the particle injection in the discrete phase model and run the simulation of the entire flow field when the particles were

included. The continuous phase (water) was still modeled as stationary, still with a second-order upwind method in order to achieve good accuracy. The discrete phase was modeled unsteady. The simulations were run with time steps of 0.005 seconds for the discrete phase until a total time of 2 seconds. The end time for the simulations was chosen on the basis of the fact that the solution did not change any more when it was carried out for longer time, i.e. the solution was steady. See Chapter 6.1.4 for details about the control of time independency. All settings for the DPM and the injection of droplets that are constant for all investigations are presented in Table B.3 and Table B.4, respectively.

5.4.1 Investigated Aspects

Several aspects of the performance of the CTC are investigated. Before the results regarding performance of the CTC are presented, some aspects regarding validity of the model are presented and discussed. Regarding the results achieved, the first thing of interest was to investigate the coalescence performance for different sizes of the droplets at the inlet. This investigation is done when both coalescence and break-up is included, and also when just coalescence is included. These results are compared and discussed. All further simulations were done with both coalescence and break-up modeling. The next investigation was to study the impact of the volume fraction of the dispersed phase. The volume fraction was varied from 1% to 7%. Another investigation was done with some other liquids with different density, viscosity, and droplet surface tension as the dispersed phase. An overview of the investigations and the parameters that are varied in the different cases is presented in Table 5.1. Please consult Table A.1 for a full presentation of all simulations.

	Coalescence/ Break-up?	**Droplet liquid**	**Volume fraction**	**Inlet diameter (μm)**
Case 1	Only coalescence	Diesel	5% for all simulations	20, 40, 60, 80, 100, 120, 140, 160, 180, 200
Case 2	Coalescence and break-up	Diesel	5% for all simulations	20, 40, 60, 80, 100, 120, 140, 160, 180, 200
Case 3	Coalescence and break-up	Diesel	1%, 3%, 5%, 7%	100 for all simulations
Case 4	Coalescence and break-up	n-Pentane, Diesel, Gas oil, Fuel oil	5% for all simulations	100 for all simulations

Table 5.1: Overview of the variable parameters in the investigations.

The performance of the CTC is mainly recognized by its ability to increase the mean diameter of the droplets during their transport through the device. This is, of course, a result of the coalescence process. A coupled parameter is the ability to migrate the droplets into the middle of the device, which will make it easier to for the droplets to coalesce. In all investigations the mean diameter used for comparison is the Sauter Mean Diameter, d_{32}. This is defined as the diameter of a sphere that has the same volume/surface area ratio as a particle of interest. It is a common measure in fluid dynamics for estimating the average particle size. The relation for the general mean diameter d_{jk} is defined as:

$$\left(d_{jk}\right)^{j-k} \equiv \frac{\int_0^\infty d^j f(d) dd}{\int_0^\infty d^k f(d) dd} \tag{5.2}$$

The distribution function, *f(d)*, is equal to the total number of droplets when it is integrated from 0 to ∞. Hence, the Sauter Mean Diameter, d_{32}, can be expressed as:

$$d_{32} = \frac{\sum N_i {d_i}^3}{\sum N_i d^2} \tag{5.3}$$

N_i is the number of droplets in the domain *i.*

6 Results and Discussion

The purpose of this Master's thesis was, as mentioned, to make a model for simulating coalescence of dispersed oil droplets in continuous water flow. The making of a model of the Compact Tubular Coalescer (CTC) did this. Hence, there were several aspects of interest. The validity and accuracy of the model is of great interest, and regarding the performance of the device the increase of mean diameter from the inlet to the outlet is crucial. The following chapters present and discuss the results achieved. All diagrams are plotted with black dots for each simulated result, and a dark red trend line is added in order to see the trend of the results.

6.1 Validity of the Model

When performing CFD-simulations it is important to evaluate the validity of the simulations. There are several aspects of the simulations that can tell us something about how accurate and valid the achieved results are. This work has focused on four things: grid independency, converged residuals, mass flow balance, and time independency. Grid independency means that the results are relatively constant even if the simulations are done on a mesh with smaller computational cells. Converged residuals mean that the residuals reach a value that is smaller than the selected convergence criterion. This means that solutions vary with a "small enough" value between the last iterations. Mass flow balance is a control of that the same amount of water that enters the device, must also come out on the other side, i.e. $\dot{m}_{water,in} = \dot{m}_{water,out}$. Time independency is checked in order to control convergence of the discrete phase since it is simulated as unsteady. The control consists of checking that the solution does not vary anymore as the simulation is iterated for more time steps.

All validation simulations are done with a test case with droplets of size 100 µm with only coalescence included (not break-up), a volume fraction of 5 %, and liquid diesel as dispersed phase, except from the mass flow balance evaluation where all simulations are considered. All other properties and parameters are equal to those that are constant for all simulations during this study.

6.1.1 Grid Independency

Six simulations of the exact same case, but with six different cell sizes were done in order to check the dependency of the grid. The overall Sauter Mean Diameter (SMD), d_{32}, for the whole domain was selected as comparing parameter between the different simulations, while the case with the finest grid was chosen as reference. The results of this test are presented in Table 6.1 and in Fig. 6.1.

Number of cells	Time for simulation	Mean diameter, d_{32}	Deviation
221512	Approx. 5 hours	203.50 µm	0 %
176205	Approx. 3 hours	203.99 µm	0.24 %
141568	Approx. 2.5 hours	210.59 µm	3.49 %
112787	Approx. 2 hours	214.24 µm	5.28 %
63655	Approx. 1 hours	228.50 µm	12.29 %
32375	Approx. 0.5 hours	247.56 µm	21.65 %

Table 6.1: Comparison between six meshes with different cell sizes.

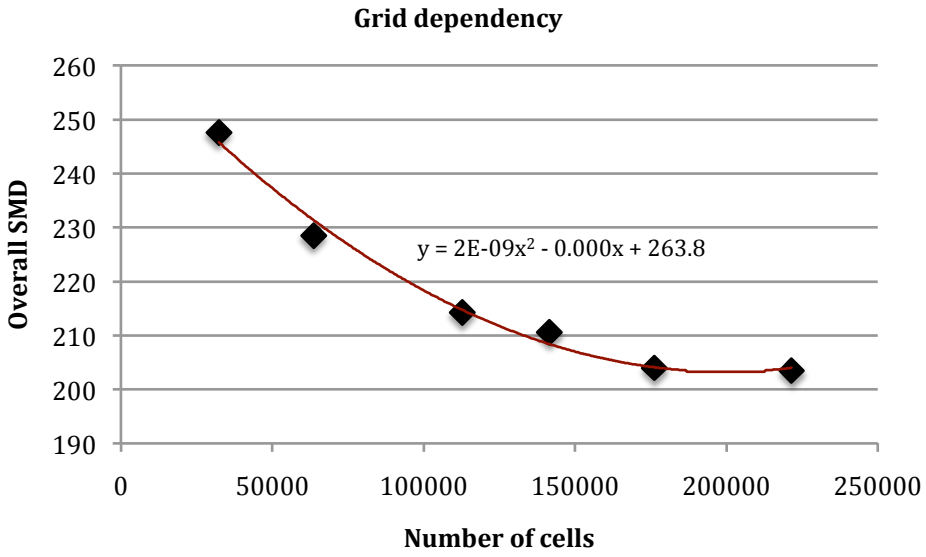

Fig. 6.1: Visualization of how the result varies with cell sizes.

One can see that the deviation decreases as the number of cells in the grid is increased. The trend line that flattens out when the number of cells is increased visualizes this. For the two cases with largest amount of cells the deviation lies beneath 1 %, which is quite acceptable. The solution of the four grids with the largest cell size are varying too much compared with the one with the smallest cell size, and can not be considered as grid-independent. Because the mesh with the smallest cell size is the most time-consuming this mesh is not preferable. Thus, the grid with 176205 cells is chosen since the result is within the acceptable deviation limit and it is not very time consuming (around 3 hours for one simulation).

6.1.2 Convergence of Residuals

As mentioned, the water phase was iterated until convergence of the residuals, first for first-order upwind method and secondly for second-order upwind method. This was done without introduction of the oil droplets. Thus, a converged, stationary solution was achieved before the droplets were introduced. The convergence criteria for all residuals were 10^{-3}. They are presented in Fig. 6.2.

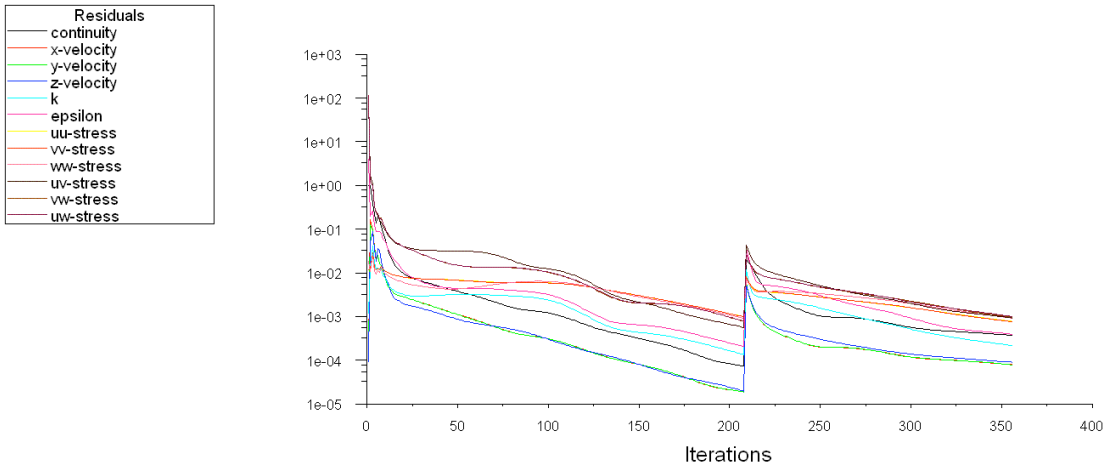

Fig. 6.2: Converged residuals for stationary solution of the water phase.

After introducing the oil droplets the residuals increases a bit before they flat out and becomes totally stable (the largest at around 10^{-2}) (Fig. 6.3). The stabilizing happens when the time stepping has reached the time for the droplets to pass through the whole device. Even though the residuals do not decrease, the solution can still be valid since the residuals are very stable and at a quite low value. Thus, other convergence controls like the mass flow balance and time independency should be evaluated in order to make a conclusion about the accuracy and validity of the solution.

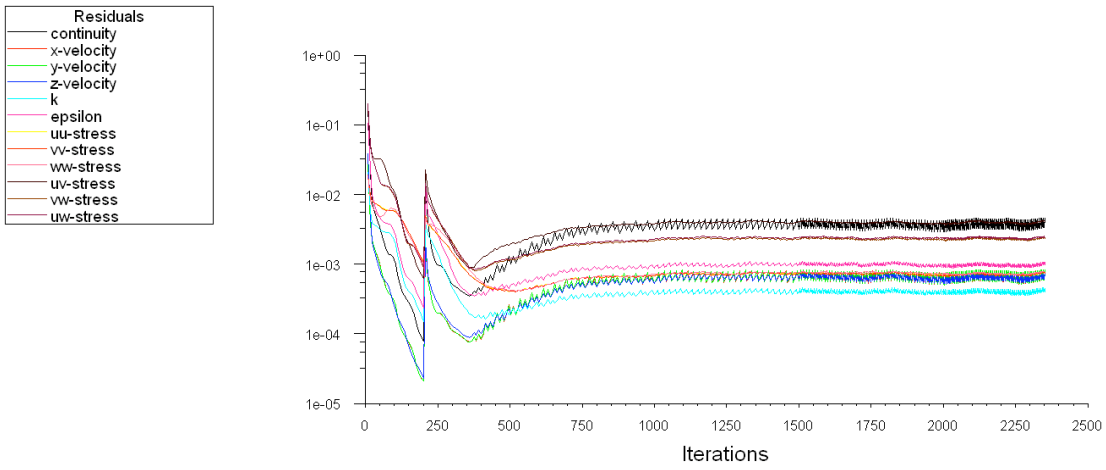

Fig. 6.3: Residuals for solution of water phase after introduction of droplets.

6.1.3 Mass Flow Balance

The mass flow balance ratio, defined as $\frac{\dot{m}_{water,out}}{\dot{m}_{water,in}}$ for all simulations are presented in Table 6.2. See Table A.1 for details about each case number.

Case number	Mass flow balance ratio
1	0.999853
2	1.000132
3	0.999869
4	1.000458
5	1.000116
6	1.000456
7	0.999991
8	0.999456
9	1.000463
10	1.000048
11	1.000194
12	1.000056
13	0.999615
14	0.999626
15	0.999978
16	0.999668
17	1.000011
18	0.999540
19	1.000204
20	0.999789
21	1.000014
22	0.999737
23	0.999453
24	0.999448
25	0.999974
26	1.000169

Table 6.2: Mass flow balance ratio for all simulations.

All values of the mass flow balance ratio are very close to 1, which means that this convergence criterion is fulfilled for all simulations. This is a good indicator for valid solutions.

6.1.4 Time Independency

In order to check if the solution remained approximately unchanged when the simulation was run for longer time, the test case was run until the total time of 3 seconds for the dispersed phase, the water phase is all the time simulated as steady. The rest of the simulations are stopped at a total time of 2 seconds. The simulation that is run until 3 seconds is chosen as reference. The result is presented in Table 6.3.

Total time	Mean diameter, d_{32}	Deviation
3 seconds	203.98 μm	0 %
2 seconds	204.13 μm	0.074 %

Table 6.3: Results of running the test case until 6 seconds.

This result shows that the change from 2 to 3 seconds is very small, under 0.1 %. This means that the solution is approximately time-independent.

The previous validation tests have shown that the model used in the simulations of this thesis is approximately both grid- and time independent, and the mass flow balance shows convergence with very small margin of error. The only

criterion that is not fulfilled, as it preferably should have been, is the convergence of the residuals after the dispersed phase is introduced. But the residuals do not in any way diverge; in fact they stabilize at a quite low value. Conclusively, with three approximately fulfilled convergence criteria and the last one not directly unfulfilled, it is basis for saying that the model is valid and quite accurate. Hence, it is a useful model for the simulations of which results follow in the next chapters.

6.2 Impact of Changing Droplet's Inlet Diameter

Ten different inlet diameters for the droplet are investigated. The Sauter Mean Diameter (SMD) for the droplets in the last quarter of the CTC is used to estimate the diameter increase of the droplets through the device. This is done because it will give a better picture of the real outlet conditions than if all droplets in the whole domain where considered. Many of these droplets are just in the beginning of their way through the device and have not been influenced by the effect of the CTC configuration. The capability of the CTC to gather the droplets in the middle of the tube is of great interest. This effect, called the migration effect, will lead to higher collision frequency and hence higher coalescence rate. The migration effect is visualized by comparing the total mass of droplets that lies inside the inner half of the cross sectional area of the CTC to the mass of droplets that are in the outer half. As for the evaluation of increase of SMD, the migration effect is also evaluated at the last quarter of the device.

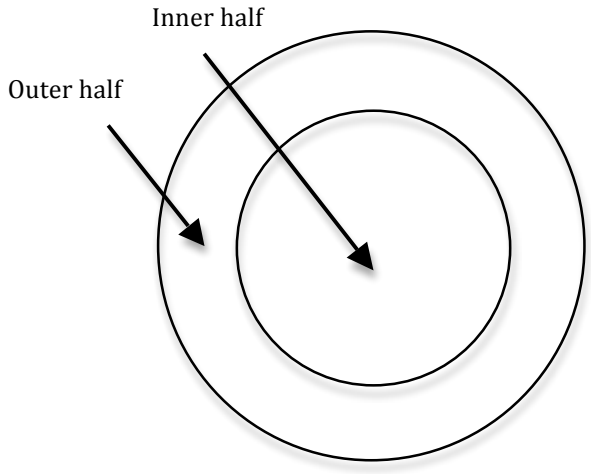

Fig. 6.4: Simplified picture of the parts of the cross sectional area of the CTC.

6.2.1 Only Coalescence Modeling

The first simulations are done with only coalescence modeling, i.e. no break-up modeling. The results regarding increase of SMD during the transport through the CTC are presented in Fig. 6.5 as percentage increase plotted against droplet inlet diameter.

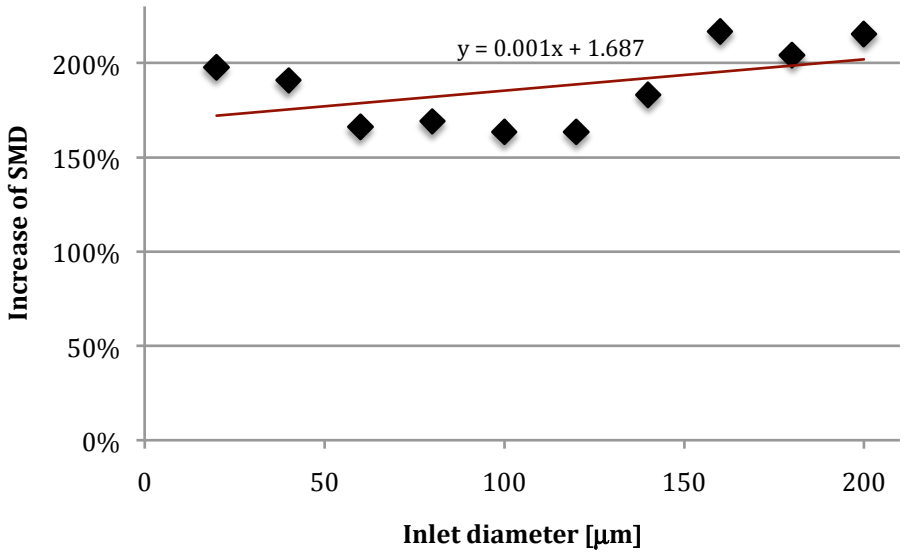

Fig. 6.5: Increase of mean droplet diameter.

By considering Fig. 6.5 one can see that the increase is quite high for all inlet diameters, from approximately 160 % up to 220 %. This observation clarifies that the coalescence process does take place and the extent of it is large enough to coalesce enough droplets with each other so that the increase of the droplets' diameter is remarkable. The diameter increase through the device is quite in the same order of magnitude for all inlet sizes, but the trend line shows a small growth in percentage diameter increase for the larger inlet diameters. This agrees with the fact shown in Fig. 6.6: that the larger droplets migrate more into the middle of the tube and increase the collision frequency. This is because the centrifugal effects have larger impact on larger particles than the smaller ones. But in a regular straight tube one would expect the coalescence rate to decrease with larger droplet sizes. This is because the total number of particles is much larger for small inlet diameters (the mass flow rate is the same); hence there are more particles that can collide/coalesce and increase the SMD.

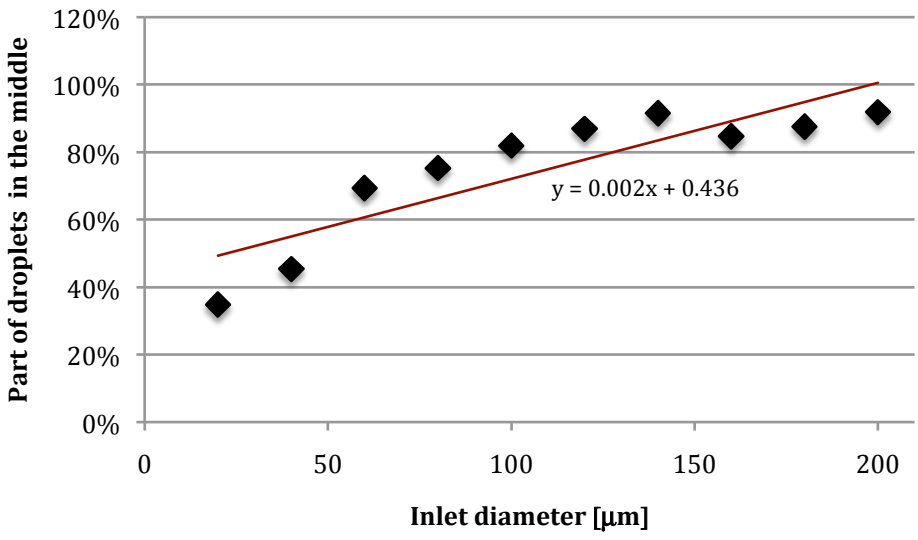

Fig. 6.6: Migration of particles into the middle of the tube.

Another argument for larger coalescence rate for smaller particles is that coalescence as a result of droplet collision is, as discussed in chapter 2.2 and 4.3, most probable for small values of both the Weber number and the impact parameter. It can clearly be seen from Fig. 6.7 that the particles' average Weber number increases (approximately linearly) when the droplet diameter increases.

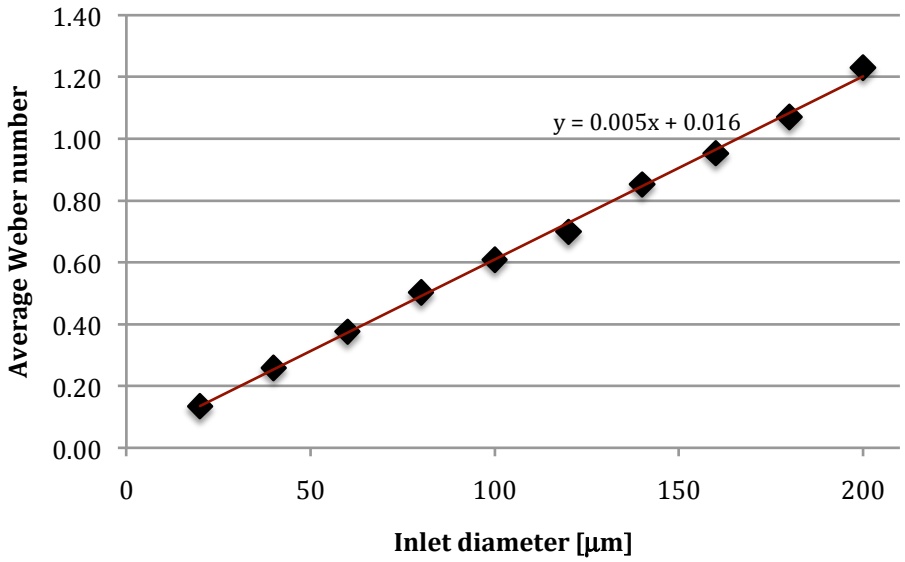

Fig. 6.7: Average Weber number for only coalescence modeling.

Although, as discussed, the trend is that the coalescence rate and increase of SMD increases slowly with the increase of inlet diameter. This shows that the increasing effect of the CTC with increasing inlet diameters is able to counteract the decreasing effect the physics of the coalescence phenomenon has on the coalescence rate for larger particles.

6.2.2 Both Coalescence and Break-up Modeling

In order to be able to make a more realistic simulation of what will happen in the CTC, both the coalescence phenomenon and the opposite break-up phenomenon need to be modeled. The next simulations are carried out with the use of FLUENT's break-up model for low Weber number flows, the TAB model. The results regarding SMD of the droplets at the end of the tube are presented in Fig. 6.8.

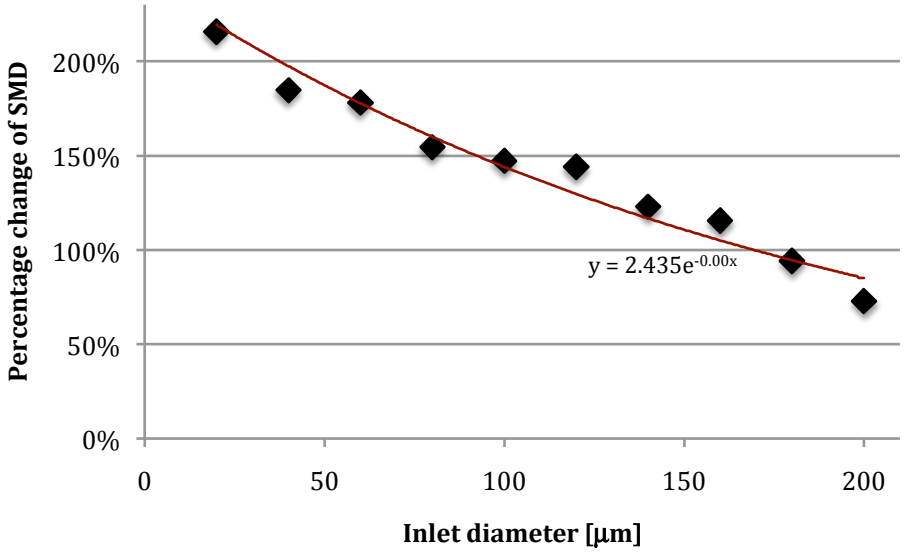

Fig. 6.8: SMD when break-up modeling is included.

The results from this simulations show, as for the modeling with no break-up, that there is a remarkable increase of the SMD for all tested inlet diameters, from approximately 70 % up to 220 %. But, unlike the results for the simulations with no break-up modeling, the percentage increase of SMD diminishes as the inlet diameters are increased. This observation is supported by the theory about break-up discussed in Chapter 2.3. For break-up to occur, a critical value of the Weber number, $(N_{We})_{crit}$, exists. If the value of the actual Weber number does not pass this critical value, break-up will not occur. By relating the droplet diameter to this critical Weber number, a critical diameter, d_{crit}, was found. Hence the droplet diameter is directly linked to the probability of break-up, and larger droplet diameters increase the probability of break-up. But even though the break-up rate is larger for the larger droplets, the coalescence rate is even larger. This is because of the centrifugal flow pattern the CTC makes. The resulting SMD at the outlet has increased with a minimum of 70 % (for the largest droplets) from the inlet. Fig. C.1 – C.5 show contours of the concentration of the dispersed phase for five different inlet diameters in a longitudinal cross sectional area of the CTC.

The average Weber number for the droplets in the CTC is presented in Fig. 6.9. Compared to the results with no break-up modeling the increase of Weber number with the inlet diameter flattens out for larger inlet sizes. The droplet Weber number is, as discussed, strongly coupled with the diameter of the droplets. Thus, the increasing break-up rate for larger droplets causes stagnation of the increase of the SMD and the droplet Weber number.

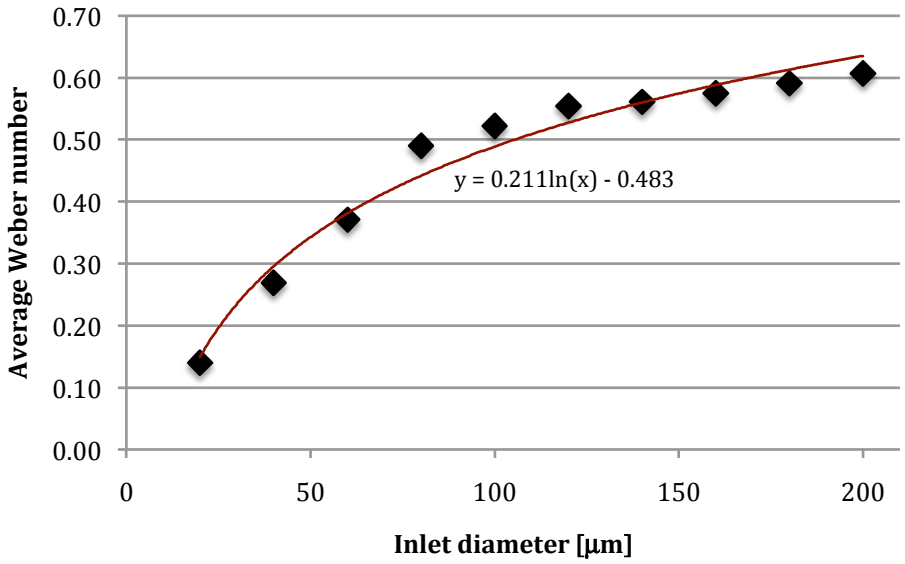

Fig. 6.9: Average Weber number for both coalescence and break-up modeling.

As observed from the previous results, the droplets' diameters increase more and more due to coalescence (more than break-up) as the droplets travel through the device. This is visualized in Fig. 6.10 where the diameters of all droplets (or parcels that FLUENT works with, c.f. chapter 4.2) are plotted as a function of the distance traveled through the tube. The result can be approximated with a trend line that shows linear increase of the droplets' diameters as they travel through the tube. This is also visualized in Fig. 6.11 where the droplets are presented and they are colored by the size of the droplets' diameters.

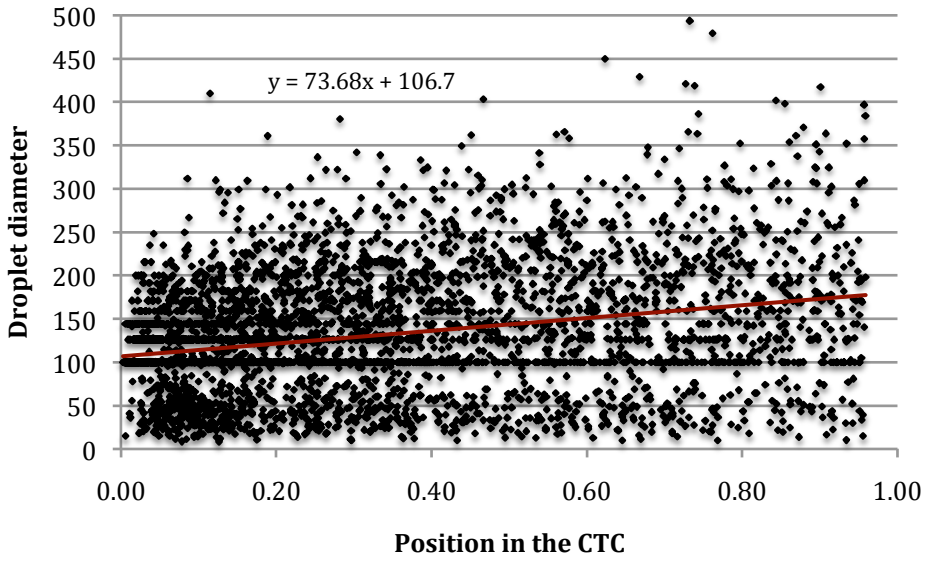

Fig. 6.10: Increase of diameter throughout the CTC.

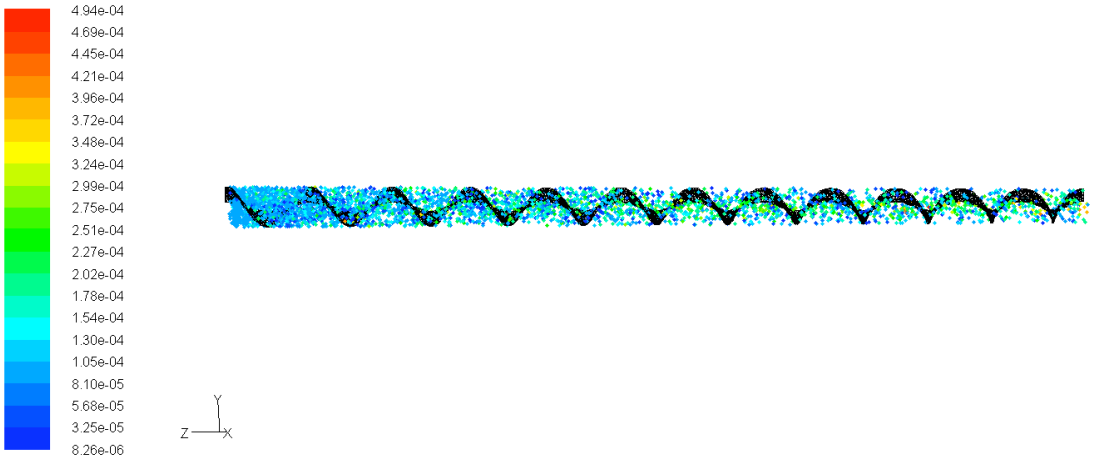

Fig. 6.11: Visualization of droplets and their diameter inside the CTC.

6.3 Impact of the Dispersed Phase Volume Fraction

Four different inlet volume fractions were investigated in order to see if this parameter had some impact on the performance of the CTC. The results obtained are presented in Fig. 6.12.

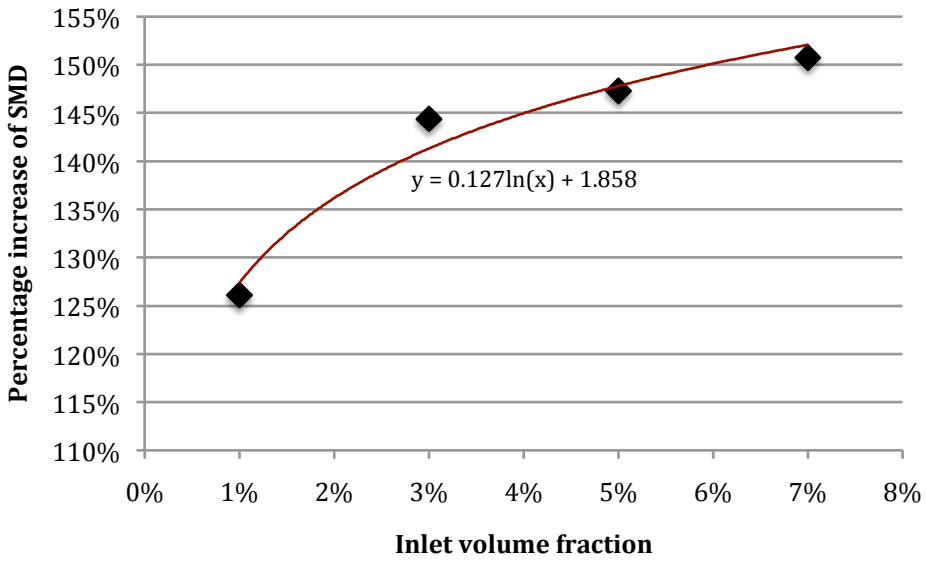

Fig. 6.12: Increase of mean droplet diameter for different volume fractions.

The coalescence process takes to a larger extent place for higher volume fractions than for the lower ones. This coincides with the expected results; when there are more droplets in the domain the change of collision increases. This can be explained by looking at the theory of collision volumes (defined bye Eq. (4.14)). When the concentration of droplets are large, the amount of collision volume is large, thus the probability of one droplet to be in the collision volume of another droplet is larger. Hence, the probability of collision and coalescence is larger.

6.4 Impact of the Type of Droplet Liquid on the Migration

The last investigation was to evaluate the effect on the CTC performance by changing the type of liquid for the droplets. Four different liquids are investigated: n-pentane, diesel, gas oil, and fuel oil. These oils have different material properties; n-pentane is the lightest, while fuel oil is the heaviest, most viscous oil. This testing is done with inlet diameter of 100 μm and a volume fraction of 5 % for all four simulations. Table A.2 shows the material properties of the four tested types of liquid. Table 6.4 shows the results achieved for the four different droplet liquids.

Droplet liquid	Increase of SMD	Part of droplets in the middle
n-Pentane	100.91 %	86.26 %
Diesel	147.29 %	85.21 %
Gas oil	155.26 %	70.80 %
Fuel oil	265.72 %	59.66 %

Table 6.4: Performance parameters for different types of droplet liquid.

The results show a clear tendency regarding the migration of droplets into the middle of the tube: the lighter oils with lower density and viscosity migrate more into the middle of the tube. Lower density ratio between the oil and the water makes the centrifugal forces more effective on the water. The heavier water is pulled away from the center of the tube due to the centrifugal flow pattern. But on the other hand, the results show that the increase of SMD is larger for the heaviest oils. This contradicts with the fact that the lightest oils gather more in the middle of the tube increase the collision frequency. But there are some considerable differences in the other physical properties: viscosity and droplet surface tension. Increased viscosity leads to increased Weber number between the droplet und the surrounding fluid, which further leads to reduction of the break-up rate. As one can see from Table A.2, the viscosity is much larger for the heavier oils. The other property that differs between the different liquids is the droplet surface tension. This parameter is included in the expression for the Weber number between the droplets. Larger droplet surface tension leads to smaller values of this Weber number, which further leads to increased coalescence rate. Thus, decreased break-up rate combined with increased coalescence rate makes the increase of SMD largest for fuel oil, even though the migration effect is lowest for this liquid.

6.5 Limitations and Weaknesses of the Model

It should be remarked that a CFD model does very often have the possibility to be better, more accurate and more applicable. This requires a lot of testing and modification, and this process is very time consuming. The time available for this Master's thesis did not allow for more work on the model than what is presented in the previous chapters. Nevertheless it is very important to be aware of what weaknesses and limitations the present model does have. Hence a short discussion of this subject follows.

Chapter 6.1.2 showed that convergence for the residuals after the dispersed phase injection was introduced was not reached. Still, a stable value was reached,

so no divergence occurred. Only 5 iterations for the continuous phase per iteration for the discrete phase were allowed. A closer look at the residuals shows that the residuals' values were decreasing during the 5 iterations between the iterations of the discrete phase, but down to values below 10^{-3} for all residuals. Allowing even more iterations for the continuous phase between the discrete phase iterations would probably resulted in more acceptable values for the residuals.

The test of grid independency in chapter 6.1.1 was done for six grids with different cell sizes. The tests showed that the difference of the test parameter between the chosen grid and the grid with smallest cells was very small; increasing the number of cells with around 25 % did not change the result with more than 0.24 %. This was a good indicator of grid independency. But it should be remarked that this test was only done with coalescence modeling, and only one parameter was tested for grid independency. Although this was the main result of interest, some other results should have been checked for the different grids in order to be more certain of grid independency. In addition, only one type of grid was tested, so ideally some other grid types should also be tested to check for grid independency.

The time step used for the unsteady simulation of the dispersed phase (Δt=0.005 s) was relatively large, and should have been tested with lower values in order to check that the solution is not time-step dependent.

Regarding applicability of the model, it should be mentioned that the model is based on FLUENT's built in model for dispersed phase flow, the discrete phase model (DPM). This model has a serious limitation when it comes to the volume fraction of the dispersed phase. The dispersed phase has to be sufficiently dilute; its volume fraction should not exceed 10 % (Fluent Inc., 2006).

6.6 Suggested Improvements of the Model

Experiences done by the simulations in this work show that the model used may, without fundamental changes, be tested more and eventually improved. As discussed above, some more testing and modification of computational parameters should be done in order to get more certain validation of the model. More time should also be spent on optimizing the model regarding both accuracy and efficiency. The model should be as computationally inexpensive as possible without loosing accuracy. The grid was equidistant and not refined in any areas. Thus, the mesh can be modified and refined in important areas of the flow field, i.e. in areas with high concentration of droplets and close to walls, and coarsened in less important areas. FLUENT provides the opportunity to adapt the grid easily in areas like this (where the concentration of the dispersed phase is large). The time step for the unsteady simulation of the dispersed phase was also discussed in the previous section, and this should be lowered in order to check for and avoid time-step dependent solution. The computational time of the present model is not very long and expensive compared to many other CFD simulations. Thus, a refining of the mesh and a lowering of the time step, which

will increase the computational time dramatically, should be tested in order to eventually obtain a more accurate and reliable solution of the problem.

7 Conclusion

The results of the simulations showed that the model is able to predict the performance of the CTC and the coalescence process of oil droplets of some different oils. The change of SMD of the droplets is the important parameter regarding the performance of the device and was thus investigated.

All cases with different inlet droplet diameters resulted in increase of the SMD, ranging from around 70 % to 220 % increase. The increase was largest for the smallest inlet diameters and smallest for the largest inlet diameters. The results showed that the configuration of the CTC was very effective. The droplets are gathered in the middle of the tube and the collision frequency is increased. When no break-up modeling was included the increase of SMD was larger for large inlet droplets. The discussion in Chapter 6.2 concluded that one would expect larger droplets to have a lower coalescence rate than the smaller ones.

Inclusion of break-up modeling, which is necessary to get a realistic simulation, resulted in lower increase of SMD for large droplets (>60-80 μm). According to the discussion in Chapter 6.2 this was expected, because the probability of break-up increases with the diameters of the droplets. Even though the inclusion of break-up resulted in lower performance of the CTC, the performance was still very good for the smallest particles (SMD increase around 200%) and acceptable for the largest particles (SMD increase around 70%).

Other simulations resulted in the conclusion that larger volume fractions of the dispersed phase generate higher increase of the SMD. The physical properties of the droplet liquid were found to be a very important factor on the CTC performance. Oils with high viscosity and large droplet surface tension had a high coalescence rate, even though the migration effect was low.

The study of the validation of the simulated results shows that the model delivers results that are, according to several controls, both quite accurate and valid. Several validation controls are done. Almost all tests gave satisfying results, but some more tests and some modification should be done in order to increase validity and accuracy. Some limitations were pointed out; in addition to the problem with the break-up modeling the model missed the applicability of handling dispersed phase volume fractions larger than 10 %.

8 Suggestions for Future Work

Additional work within the problems discussed in this work should first of all concentrate on improvement of the mathematical model developed. As discussed in chapter 6.5 and 6.6 the model should undergo some more testing to ensure that it is grid independent and time-step independent, i.e. adaption of the grid and reduction of the time step for particle tracking. More time should also be used on optimizing the model regarding both accuracy and efficiency in order to get a model that is as economic as possible within the frames of acceptable accuracy.

Secondly, some other aspects of the model should be tested. This may be testing of the effect of changing the diameter and length of the CTC. What must the length of the device be if the diameter is increased in order to have the same performance? Also, it would still be interesting to check the performance of he CTC on even more kinds of oils, and also other media as continuous phase. The model should also be tested for more realistic inlet distributions than the uniform distribution used in this study.

It would also be interesting to see the result of another approach for the same case of study, e.g. a Eulerian approach. This is a multiphase model provided in FLUENT. In order to model coalescence and break-up with this approach, the theory of population balances must be included. There exist a purchasable add-on module for the latest version of FLUENT, which includes population balance modeling. This approach will not have the same limitation regarding the volume fraction of the dispersed phase.

Appendix A, Overview of Simulations and Liquid Properties

Table A.1 and A.2 contain an overview of all performed simulations and the properties of all used liquids, respectively.

Case number	Coalescence modeling	Break-up modeling	Droplet liquid	Volume Fraction	Inlet diameter
1	Yes	No	Diesel	5%	20 µm
2	Yes	No	Diesel	5%	40 µm
3	Yes	No	Diesel	5%	60 µm
4	Yes	No	Diesel	5%	80 µm
5	Yes	No	Diesel	5%	100 µm
6	Yes	No	Diesel	5%	120 µm
7	Yes	No	Diesel	5%	140 µm
8	Yes	Yes	Diesel	5%	160 µm
9	Yes	Yes	Diesel	5%	180 µm
10	Yes	Yes	Diesel	5%	200 µm
11	Yes	Yes	Diesel	5%	20 µm
12	Yes	Yes	Diesel	5%	40 µm
13	Yes	Yes	Diesel	5%	60 µm
14	Yes	Yes	Diesel	5%	80 µm
15	Yes	Yes	Diesel	5%	100 µm
16	Yes	Yes	Diesel	5%	120 µm
17	Yes	Yes	Diesel	5%	140 µm
18	Yes	Yes	Diesel	5%	160 µm
19	Yes	Yes	Diesel	5%	180 µm
20	Yes	Yes	Diesel	5%	200 µm
21	Yes	Yes	Diesel	1%	100 µm
22	Yes	Yes	Diesel	3%	100 µm
23	Yes	Yes	Diesel	7%	100 µm
24	Yes	Yes	n-Pentane	5%	100 µm
25	Yes	Yes	Gas oil	5%	100 µm
26	Yes	Yes	Fuel oil	5%	100 µm

Table A.1: Presentation of all simulations.

Droplet liquid	Chemical Notation	Density (kg/m^3)	Viscosity (kg/ms)	Droplet Surface Tension (N/m)
n-pentane	C_5H_{12}	626.0	0.000229	0.015508
Diesel	$C_{10}H_{22}$	730.0	0.002400	0.026326
Gas oil	$C_{16}H_{29}$	830.0	0.003320	0.019036
Fuel oil	$C_{19}H_{30}$	960.0	0.048000	0.030000
Water	H_2O	998.2	0.001030	-

Table A.2: Material properties for the different liquids used in the study.

Appendix B, Settings used in FLUENT

Table B.1 – B.4 present a complete overview of all settings used for the simulations in FLUENT.

Category	Sub-Category 1	Sub-Category 2	Choice/Value	Choice/Value
MODEL	Solver	Solver Formulation Time Space Gradient	Pressure Based Implicit Steady 3D Green-Gauss Cell Based	
	Energy		OFF	
	Viscous	Model Reynolds-Stress Model Reynolds-Stress Options Near-Wall Treatment Model Constants	Reynolds Stress Linear Pressure-Strain Wall BC from k Equation Wall Reflection Effects Standard Wall Functions Default values for all constants	
	Radiation		OFF	
OPERATING CONDITIONS	Pressure	Operating Reference Pressure	101325 Pa x=0, y=0, z=0	
	Gravity		Gravitational Acceleration	x=0 m/s^2, y=-9.81 m/s^2, z=0 m/s^2
BOUNDARY CONDITIONS	Default	Interior		
	Fluid	Fluid	Water (liquid)	Default values
	Inducer	Wall	Default values	
	Inlet	Velocity-inlet	Velocity Magnitude Turb. Kinetic Energy Turb. Diss. Rate K and Turb. Intensity Discrete Phase BC Type	2 m/s 0.3 m^2/s^2 1 m^2/s^3 Escape
	Outer Wall	Wall	Default values	
	Outlet	Pressure Outlet	Gauge Pressure Turb. Kinetic Energy Turb. Diss. Rate K and Turb. Intensity Discrete Phase BC Type	101325 Pa 0.3 m^2/s^2 1 m^2/s^3 Escape

Table B.1: Settings for the simulations of the water phase in FLUENT.

Category	Choice/Value	Choice/Value
Equations	Flow, Turbulence, Reynolds Sresses	
Pressure-Velocity Coupling	SIMPLE	
Under-Relaxation Factors	Pressure Density Body Forces Momentum Turb.Kin. Energy Turb. Diss. Rate Turb. Viscosity Reynolds Stresses Disc. Pha. Sources	0.3 1 1 0.7 0.8 0.8 1 0.5 0.5
Discretization	Pressure Momentum Turb. Kin. Energy Turb. Diss. Rate Reynolds Stresses	Standard 2. order upwind 2. order upwind 2. order upwind 2. order upwind

Table B.2: Settings for the solution controls in FLUENT.

Category	Sub-Category 1	Sub-Category 2	Choice/Value	Choice/Value
DISCRETE PHASE MODEL	Interaction	Interaction with continuous phase	ON	
		Update DPM Sources Every Flow Iteration	OFF	
		Number of Continuous Phase Iterations per DPM Iteration	10	
	Particle Treatment	Unsteady Particle Tracking	ON	
		Particle Time Step Size	0.005 s	
		Number of Time Steps	1	
	Tracking	Tracking Parameters	Default values	
		Drag Parameters	Default values	
	Physical Models	Options	Default values	
		Spray Model	Droplet Collision Droplet Breakup	See Table 5.1 See Table 5.1
	Numerics	Options	Default values	
		Tracking Scheme Selection	Default values	

Table B.3: Settings used in the DPM in FLUENT.

Category	Sub-Category	Choice/Value	Choice/Value
Injection Type	Surface		
Release From Surfaces	Inlet		
Particle Type	Inert		
Material	See Table 5.1		
Diameter Distribution	Uniform		
Point Properties	X-velocity	0 m/s	
	Y-velocity	0 m/s	
	Z-velocity	-2 m/s	
	Diameter	See Table 5.1	
	Start Time	0 s	
	Stop Time	10 s	
	Total Flow Rate	See Table 5.1	
Turbulent Dispersion	Stochastic Tracking	Discrete Random Walk Model	ON
		Random Eddy Lifetime	OFF
		Time Scale Constant	0.15

Table B.4: Settings for the injection used in the DPM in FLUENT.

Appendix C, Visualization of Dispersed Phase Concentration

Figure C.1 – C.5 presents contours of the droplet concentration in five cases with different inlet diameter of diesel droplets.

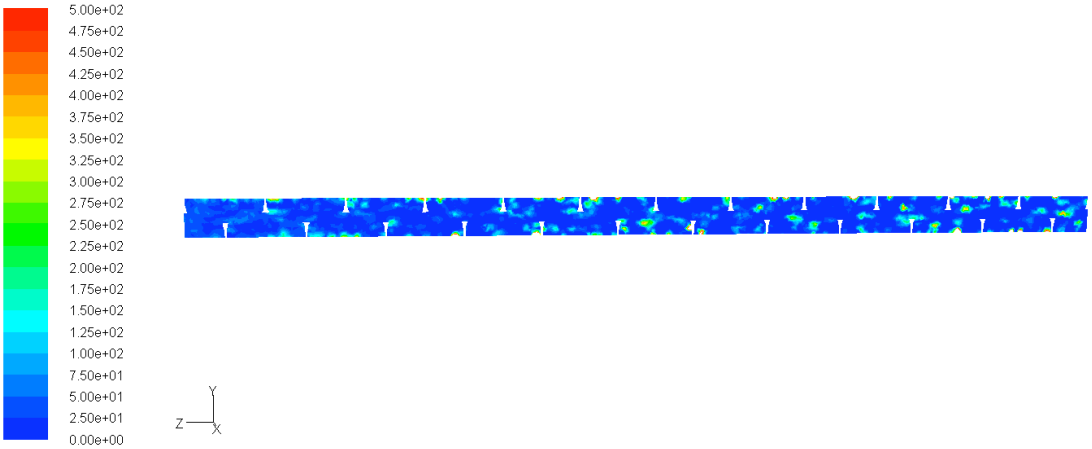

Fig. C1: Contours of DPM concentration, inlet diameter of 20 µm (kg/m³).

Fig. C2: Contours of DPM concentration, inlet diameter of 60 µm (kg/m³).

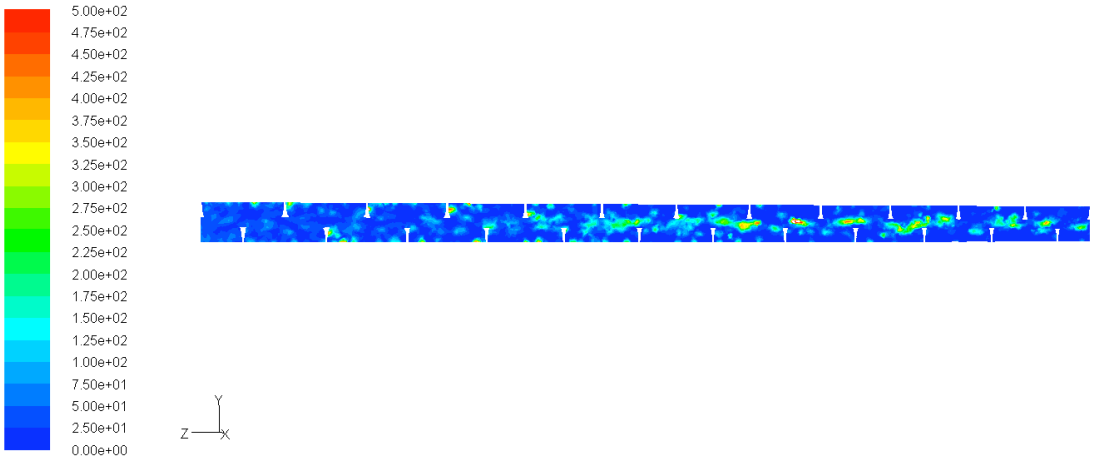

Fig. C3: Contours of DPM concentration, inlet diameter of 100 µm (kg/m³).

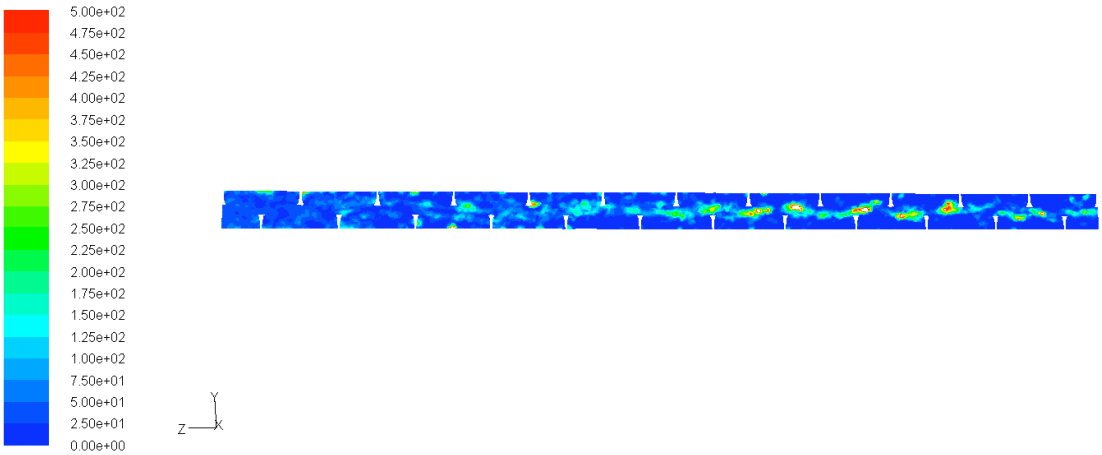

Fig. C4: Contours of DPM concentration, inlet diameter of 140 µm (kg/m³).

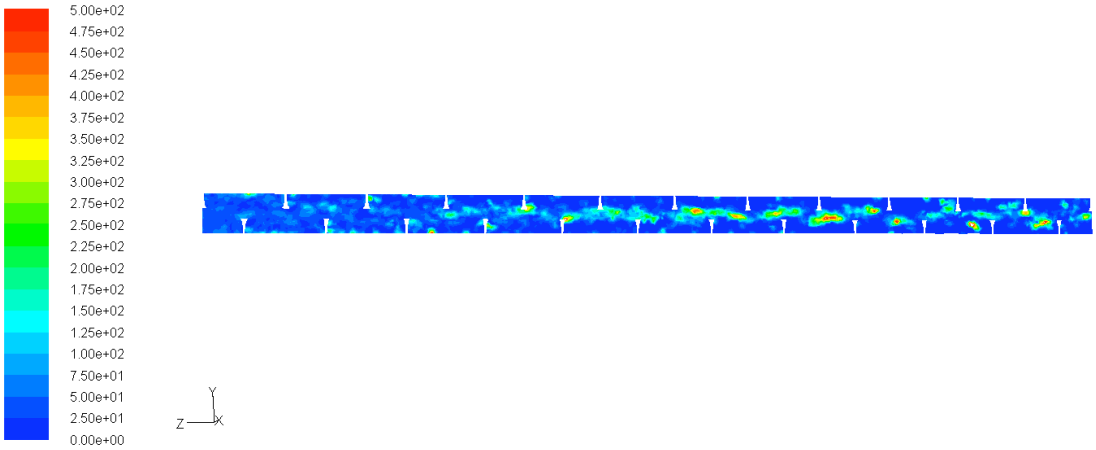

Fig. C5: Contours of DPM concentration, inlet diameter of 180 µm (kg/m³).

List of References

1. Ashgriz, N., & Poo, J. Y. (1990). Coalescence and separation in binary collisions of liquid drops. *Journal of Fluid Mechanics , 221*, 183-204.

2. Dhainaut, M. (2002). *Literature Study on Observation and Experiments on Coalescence and Breakup of Bubbles and Drops.* SINTEF, Materials Technology. SINTEF.

3. Elgobashi, S. (1991). Particle-laden turbulent flows: direct simulation and closure models. *Applied scientific research , 48* (3), 301.

4. Fluent Inc. (2006). *FLUENT 6.3 User's Guide.* Fluent Inc.

5. Haider, A., & Levenspiel, O. (1989). Drag Coefficient and Terminal Velocity of Spherical and Nonspherical Particles. *Powder technology , 58* (1), 63-70.

6. Hinze, J. (1955). Fundamentals of the Hydrodynamic Mechanism of Splitting in Dispersion Processes. *AIChe Journal , 3* (1), 289-295.

7. Ko, G. H., & Ryou, H. S. (2005). Modeling of droplet collision-induced breakup process. *International Journal of Multiphase Flow , 31* (6), 723-738.

8. Müller, B. (2007). Introduction to Computational Fluid Dynamics. *Introduction to Computational Fluid Dynamics* .

9. Mashayek, F., Ashgriz, N., Minkowycz, W., & Shotorban, B. (2003). Coalescence collision of liquid drops. *International Journal of Heat and Mass Transfer , 46* (1), 77-89.

10. Morsi, S., & Alexander, A. (1972). An Investigation of Particle Trajectories in Two-Phase Flow Systems. *Journal of Fluid Mechanics , 55* (SEP26), 193-208.

11. O'Rourke, P. (1981). *Collective drop effects on vaporizing liquid sprays.* Thesis, Los Alamos National Lab., NM (USA).

12. Prince, M. J., & Blanch, H. W. (1990). Bubble coalescence and break-up in air-sparged bubble columns. *AIChE Journal , 36*, 1485-1499.

13. Ramkrishna, D. (2000). *Population balances : theory and applications to particulate systems in engineering.* San Diego: Academic Press.

14. van Leer, B. (1977). Towards the Ultimate Conservative Difference Scheme. IV. A New Approach to Numerical Convection. *J. Comput. Phys.*

15. Versteeg, H., & Malalasekra, W. (1995). *An Introduction to Computational Fluid Dynamics: The Finite Volume Method.* Harlow, England: Pearson Education Limited.

16. White, F. M. (2003). *Fluid Mechanics.*